Prevalent and Dynamic Binding of the Cell Cycle Checkpoint Kinase Rad53 to Gene Promoters

Yi-Jun Sheu, Risa Karakida Kawaguchi, Jesse Gillis and Bruce Stillman[1]

Cold Spring Harbor Laboratory, 1 Bungtown Road, Cold Spring Harbor, NY 11724, USA

Current addresses:
Jesse Gillis: Department of Physiology, Donnelly Centre, University of Toronto, 160 College Street, Room 230, Toronto, Ontario CANADA M5S 3E1
Risa Karakida Kawaguchi: Center for iPS Cell Research and Application, Kyoto University, 53 Kawahara-cho, Shogoin, Sakyo-ku, Kyoto 606-8507, Japan

[1]Correspondence: Bruce Stillman stillman@cshl.edu

Key words: Origins of DNA replication, Transcription start sites, Gene promoters, Checkpoint Kinase, Rad53, DNA damage response, Stress Response

Abstract

Replication of the genome must be coordinated with gene transcription and cellular metabolism, especially following replication stress in the presence of limiting deoxyribonucleotides. The *S. cerevisiae* Rad53 (CHEK2 in mammals) checkpoint kinase plays a major role in cellular responses to DNA replication stress. Cell cycle regulated, genome-wide binding of Rad53 to chromatin was examined. Under replication stress, the kinase bound to sites of active DNA replication initiation and fork progression, but unexpectedly to the promoters of about 20% of genes encoding proteins involved in multiple cellular functions. Rad53 promoter binding correlated with changes in expression of a subset of genes. Rad53 promoter binding to certain genes was influenced by sequence-specific transcription factors and less by checkpoint signaling. However, in checkpoint mutants, untimely activation of late-replicating origins reduces the transcription of nearby genes, with concomitant localization of Rad53 to their gene bodies. We suggest that the Rad53 checkpoint kinase coordinates genome-wide replication and transcription under replication stress conditions.

Introduction

Rad53, the homolog of the mammalian CHEK2 kinase present in the budding yeast *S. cerevisiae*, is an essential kinase involved in a multitude of cellular processes. The most well-established function of Rad53 is its role as an effector kinase in response to various sources of DNA damage. To maintain genome stability during S-phase, a DNA replication checkpoint (DRC) is activated in response to replication stress via the sensor kinase Mec1 (the mammalian ATM/ATR), the replication fork protein Mrc1 (Claspin in mammals) and other fork proteins (Lanz et al., 2019; Osborn and Elledge, 2003; Pardo et al., 2017; Paulovich and Hartwell, 1995; Saldivar et al., 2017). A second DNA damage checkpoint (DDC) mediated by Rad9 (TP53BP1 in mammals) responds to double strand DNA breaks. Both branches converge on the effector kinase Rad53, which triggers a wide range of downstream events, including slowing or halting cell cycle progression, transiently preventing initiation of DNA replication at origins that have not yet replicated, activating DNA repair pathways and elevating the synthesis of deoxyribonucleoside triphosphates (dNTP) by upregulating genes encoding the ribonucleotide reductase (RNR). The checkpoint signaling also promotes widespread changes in gene expression (Jaehnig et al., 2013; Pardo et al., 2017).

Unlike most of the checkpoint genes, both Mec1 and Rad53 kinases are essential for cell viability in unperturbed cells. This can be partly explained by their role in regulating dNTP pools (Desany et al., 1998; Forey et al., 2020; Zhao et al., 2000). However, under the bypass conditions in cells without Sml1, the inhibitor of the RNR enzyme, cells lacking either kinases are viable. Yet, it is important to note that these kinase-null mutants are extremely sick and sensitive to various types of exogenous stress. Furthermore, lacking Rad53 causes a more severe defect than lacking Mec1, implying that Rad53 has activities beyond checkpoint signaling. Consistent with this suggestion, the kinase-deficient mutant *rad53*^{K227A} lacks checkpoint function but retains growth-associated activity and an additional *rad53* mutation was found that is checkpoint proficient but supports cell growth poorly (Gunjan and Verreault, 2003; Hoch et al., 2013; Holzen and Sclafani, 2010; Pellicioli et al., 1999).

Rad53 is central to the transcriptional response to DNA damage. It is well-established that the Dun1 protein kinase acts downstream of Rad53 to phosphorylate and inactivate the transcriptional repressor Rfx1/Crt1 and thereby up-regulate target genes (Huang et al., 1998), including *RNR2*, *RNR3*, and *RNR4*, encoding subunits of RNR. However, the induced expression of *RNR1*, which encodes the major isoform of the RNR large subunit, is not controlled by the Rfx1 repressor, but by Ixr1 binding to the *RNR1* promoter upon genotoxic stress (Tsaponina et al., 2011). This Ixr1-dependent regulation of *RNR1* is independent of Dun1 but requires Rad53. Another Rad53-dependent, Dun1-independent regulation of *RNR1* involves dissociation of the Nrm1 repressor from MBF following Nrm1 phosphorylation by Rad53 (Travesa et al., 2012). Thus, the Rad53-dependent transcription control is complex, but not yet fully understood.

In addition to upregulating the dNTP pools, defects in cells lacking Rad53 can be suppressed by manipulating factors functioning in transcription regulation, cell wall maintenance, proteolysis and cell cycle control (Desany et al., 1998; Manfrini et al., 2012). Moreover, Rad53 kinase targets and interaction partners found in biochemical and proteomic studies suggests that the

kinase is pleiotropic (Gunjan and Verreault, 2003; Jaehnig et al., 2013; Lao et al., 2018; Smolka et al., 2007, 2006).

In this study, while investigating the response of yeast cells to replication stresses caused by depletion of dNTPs, we found that Rad53 localized to more than 20% of gene promoters in the *S. cerevisiae* genome, suggesting a multifaceted role in coordinating stress responses. Furthermore, we provide evidence that in the absence of the DRC checkpoint pathway, untimely activation of replication from late origins can negatively affect transcription activity of nearby genes.

Results

Rad53 is recruited to genomic loci other than replication origins in proliferating yeast cells

Previous studies focusing on specific genomic features, mainly subsets of DNA replication origins, have detected Rad53 binding to replication origins and replication forks (Can et al., 2018; Dohrmann and Sclafani, 2006). However, given the evidence that Rad53 has functions beyond the control of DNA replication stress, it is possible that Rad53 also functions at additional genomic loci. We therefore investigated the genome-wide distribution of Rad53 by chromatin immunoprecipitation and deep sequencing (ChIP-seq) in proliferating yeast cells (Behrouzi et al., 2016). Since the *sml1* null mutation (*sml1Δ*) allows cells to bypass the requirement for Rad53, or its upstream kinase Mec1, for growth, we also performed ChIP-seq in the *sml1Δ* mutant and the *rad53 null* (*rad53Δ sml1Δ)* as controls for antibody specificity (Figure 1).

Visual inspection of the ChIP-Seq peaks from normalized coverage tracks suggested that Rad53 bound to sites throughout the genome (Figure 1a). Rad53 binding to the same sites also occurred in the *sml1Δ* mutant and the *mec1Δ sml1Δ* mutant, but was absent in the *rad53Δ sml1Δ* mutant. Computational analysis was performed to generate heatmaps of Rad53 ChIP-seq signal across 2 kb intervals centered on transcription start sites (TSSs) (Figure 1b). The average Rad53 ChIP-seq signal on top of the heatmap show that Rad53 was most concentrated within 500 bp upstream of TSSs in *WT*, *sml1Δ* and *mec1Δ sml1Δ* mutants. A smaller fraction of genes also have signal within the gene bodies. No Rad53 signal beyond background was detected at TSSs in the *rad53Δ sml1Δ* cells, demonstrating antibody specificity. Analysis by calculating empirical p-values for the ChIP-seq signals 500 bp upstream of TSS found that, out of 6604 genes, 1464, 1983 and 1293 in *WT*, *sml1Δ* and *mec1Δ sml1Δ*, respectively, exhibited significant Rad53 signal at this region. This represents ~20% or greater of all gene promoters.

Heatmap analysis was also performed on Rad53 ChIP-seq signal across 30 kb intervals centered on all origins annotated in the OriDB database (Siow et al., 2012). The average signal across the whole region was higher in *WT*, *sml1Δ* and *mec1Δ sml1Δ* than in *rad53Δ sml1Δ* after normalization (Figure 1c). However, the signal was not concentrated at the origins. Since these ChIP-seq datasets are from asynchronous cells, this finding is consistent with the idea that recruitment of Rad53 to replication origins is cell cycle regulated rather than constant binding to origins.

Binding of Rad53 to upstream TSS changes with cell cycle stages

To gain insight into the dynamics of Rad53 recruitment to genomic loci such as promoters and replication origins, Rad53 ChIP-seq was analyzed in samples from synchronized cell cultures. Cells were arrested in G1 using α-factor and then released into media containing hydroxyurea (HU) to induce replication stress caused by limiting dNTPs. Three stages of synchronous cell cultures were collected and referred to as G1 (for cells arrested in G1), HU45 and HU90 (for cells released from G1 into HU for 45 and 90 minutes, respectively). These cell samples were then processed for ChIP-seq analysis. Heatmaps of the Rad53 signals at 2 kb intervals centered on all transcription start sites (TSS) show a trend of increasing Rad53 binding as cells progress from G1-phase into HU45 or HU90 (Figure 2a), concomitant with increased levels of Rad53 protein in cells treated with HU (Figure 2 – figure supplement 1). The increase in Rad53 parallels entry into S-phase, as measured by Orc6 phosphorylation (Figure 2 – figure supplement 1a). Similar to the data from asynchronous cell samples, Rad53 signals were most concentrated upstream of TSSs (Figure 2a, left panel). The ChIP-Seq signals using antibodies against γ-H2A, which like Rad53 is a target of the sensor kinase Mec1, were not enriched upstream of TSSs (Figure 2a, right panel). In fact, the signals for γ-H2A were lower immediately upstream of TSSs than the surrounding regions, consistent with promoters being histone free regions.

Further analysis showed that >85 % of the Rad53 ChIP-seq peaks overlap with gene promoters (defined as 500 bp upstream and 50 bp downstream of TSS) at all stages investigated. The distribution of aggregated peak numbers around transcription start sites showed highest count numbers immediately upstream of the TSS (Figure 2b). By visual inspection of normalized ChIP-seq coverage tracks, we noticed that signals at promoters of genes such as *RNR1*, *PCL1* and *TOS6* varied depending on the cell cycle stage (Figure 2c, bottom three tracks for *WT* at stages of G1, HU45 and HU90) while signals at neighboring gene promoters remained largely constant. Thus, the recruitment of Rad53 to a subset of gene promoters is regulated. Because *RNR1*, *PCL1* and *TOS6* are known targets of the cell cycle regulator SBF, a sequence-specific transcription factor composed of subunits Swi4 and Swi6, we compared Rad53 ChIP-Seq data and a previous ChIP-Seq dataset of Swi6 (Park et al., 2013). As indicators for the gene specificity of protein binding, the Gini indices were computed from Lorenz curves of ChIP-Seq data for Swi6 and two of our Rad53 replicates (Figure 2d), being 0.763, 0.2918, and 0.2982, respectively. Rad53 has a coverage for many promoters while Swi6 shows substantially high coverage only for a limited number of promoters. Thus, it is likely Rad53 would effect a wider range of genes than the Swi6 regulatory network.

Previous studies have found that under certain conditions, regions of the genome are promiscuously present in ChIP-Seq studies independent of the antibody used (Park et al., 2013; Teytelman et al., 2013). These regions were termed hyper-ChIPable regions and were found enriched for sequences in and around gene bodies of highly expressed genes. We therefore examined whether these regions were promiscuously present under our conditions. Analysis of ChIP-Seq data for Rad53 and γ-H2A with or without the hyper-ChIPable regions observed by Teytelman et al. and Park et al. did not alter the pattern of Rad53 binding to TSSs (Figure 2 – figure supplement 2 a-d). When we specifically examined the pattern of Rad53 ChIP-Seq signals around TSSs of the 296 genes associated with those hyper-ChIPable sequences, we observed not only localization to TSSs, but also enrichment to the gene bodies as previously

reported (Park et al., 2013; Teytelman et al., 2013). This pattern is distinct from the pattern of promoter localization (compare Figure 2 – figure supplement 2 d and e). Furthermore, KEGG analysis of the genes enriched in the studies by Teytelman et al. and Park et al. showed predominantly genes encoding snoRNAs and tRNAs, genes we did not find in the promoter binding for Rad53 (Figure 2 – figure supplement 2f). Finally, we did not observe any enrichment at gene promoters when the *RAD53* gene was deleted from the strain (Figure 1, a and b) or when anti-γ-H2A antibodies were used (Figure 2a). Thus, we suggest that the Rad53 binding observed here is not the same as the promiscuous, non-specific enrichment of hyper-ChIPable regions reported previously. Moreover, Rad53 binding to a subset of promoters is transcription factor dependent (see below).

Rad53 is recruited to sites of DNA synthesis independent of checkpoint signaling

Since previous studies reported localization of Rad53 to replication origins (Can et al., 2018; Dohrmann and Sclafani, 2006), we also performed heatmap analysis of ChIP-seq signal around replication origins for Rad53, γ-H2A and Cdc45, a component of active helicase complex and hence the marker for active replication forks (Figure 2 – figure supplement 3). The 30 kb window for the heatmap around origins was chosen based on our prior knowledge that the extent of DNA synthesis in *WT* cells under similar growth conditions at HU90 was about 10 kb (Sheu et al., 2014). In *WT* cells, the Rad53 signal was present at regions associated with early firing origins but not with late firing origins that are inactive due to inhibition by the HU-induced checkpoint. However, Rad53 signal was also present at late origins in the kinase-deficient $rad53^{K227A}$ and *mrc1Δ* mutants, both of which allow activation of late origins as a result of the checkpoint defect. Thus, Rad53 was recruited only to replication forks associated with activated origins and the pattern was similar to that of Cdc45. Surprisingly, Rad53 binding to replication forks did not require Mrc1 or its own kinase activity, suggesting checkpoint-independent recruitment of Rad53 to sites of DNA synthesis.

Interestingly, γ-H2A was observed at genomic regions surrounding the very late origins in G1-phase in both *WT* and mutants (Figure 2 – figure supplement 3b). It is possible that these γ-H2A signals reflect a low level of ssDNA gaps at these late-replicating regions that was tolerated and carried over from the previous cell cycle, similar to unrepaired post-replication gaps resulting from low level of UV irradiation found in *S. pombe* G2-phase (Callegari and Kelly, 2006).

Identification of genes with differential binding of Rad53 at promoters

Rad53 promoter binding was temporally dynamic in a subset of genes, suggesting regulation by cell cycle progression or DNA replication stress. To identify genes with differential or dynamic binding of Rad53 at their promoters (DB genes), we applied residual analysis. The read count difference was investigated for the promoter regions (500 bp window upstream of TSSs) of all genes for Rad53 ChIP-seq. The comparison was done between stages G1 and HU45 of *WT* samples from two independent experiments (termed CP and TF, Figure 3a). Since each dataset had two biological replicates from stages G1 and HU45, we extracted the top 1,000 genes that displayed dynamic binding from the aggregated read coverage and called these genes the top DB genes (Figure 3a). Among the 1000 top DB genes from each set of comparison, 435 genes were identified in both sets (435 Top DB overlap).

Overall, during the G1- to S-phase transition (HU45), there are more genes with increased Rad53 promoter binding than those with decreased binding: within the list of 435 genes, 337 show increased Rad53 binding at their promoters, while 98 show decreased binding (Figure 3b). These genes include those involved in cell cycle progression (e.g., genes encoding cyclins and regulators of DNA replication) and cell growth (e. g., cell wall maintenance and mating response). Figure 3c shows Rad53 dynamic binding, either up or down, at the promoters of representative genes as cells transitioned from G1 phase to HU45 and HU90 time points.

The relationship between Rad53 promoter binding and gene expression

To gain insight into the relationship between Rad53 promoter recruitment and gene expression, RNA-seq analysis was performed under the same growth conditions used for the ChIP-seq experiments. RNA-seq replicates of datasets from 4 yeast strains (*WT*, *rad9Δ*, *rad53*^{K227A} and *mrc1Δ*), each with 3 stages (G1, HU45 and HU90) were analyzed using rank data analysis (Figure 4a). In the hierarchical clustering, cell cycle stage contributes more to similarities in expression than the genotype. In particular, the expression profiles in G1 were very similar among all strains. In HU45, however, two subgroups clustered by genotype were evident: *rad9Δ* clustered with *WT*, consistent with Rad9 having no role in the DRC checkpoint branch, while *rad53*^{K227A} and *mrc1Δ* clustered together, consistent with Rad53 and Mrc1 functioning together in the DRC response to HU stress.

Pair-wise comparisons of G1 to HU45 samples showed that, in both *WT* and *rad9Δ* cells, ~2300 genes exhibited significant expression changes (differentially expressed genes, DEGs; Figure 4b). The number of DEGs increased to ~3000 when comparing G1 to HU90. Moreover, in both *rad53*^{K227A} and *mrc1Δ* mutants, ~2500 DEGs were detected from G1 to HU45, which increased to >3400 in G1 to HU90. The response to cell cycle stage was largely equally distributed between up and down regulation. Comparison of *WT* to *rad53*^{K227A} in the HU45 and HU90 conditions found 517 and 2234 DEGs, respectively, while comparison of *WT* to *mrc1Δ* revealed 370 and 1166 DEGs in HU45 and HU90. A *WT* and *rad9Δ* comparison at all stages showed only 5 DEGs, including the deleted *RAD9* gene and its marker cassette *HIS3*. Thus, Rad9 did not contribute much to gene expression changes under HU stress.

Based on ChIP-Seq data, the average Rad53 binding upstream of TSSs was higher in the significant DEGs than in the insignificant, when comparing G1 to HU45 or to HU90 of the *WT* datasets (Figure 4c and Figure 4 – figure supplement 1a). These results suggested that Rad53 may play a role in the control of gene expression at a subset of expressed genes. Similar observations were also apparent when comparing stage-dependent samples in the checkpoint mutants (Figure 4 – figure supplement 1b and c), demonstrating that the functions of Rad53 at gene promoters were not solely checkpoint-dependent. Therefore, we performed gene co-expression analysis based on association in the co-expression network (Lee et al., 2020). Co-expression analysis of significant DEGs in *WT*(G1→HU45) yielded ten co-expression clusters (Figure 5a). Dynamic Rad53 binding at promoter regions occurred in most clusters (Figure 5b), with significantly enriched GO functions including cell cycle regulation, mating response, proteolysis, transport, oxidation-reduction process and organic acid metabolism (Figure 5a). Within the 435 Top DB overlap gene group (Figure 3b), 236 genes were also detected as DEGs

(236 DB/DEGs) in the *WT*(G1→HU45) comparison. The association between binding changes and expression changes was significant (Figure 5d, left panel; Fischer's exact test $p < 0.0001$). Plots of Rad53 binding changes against gene expression changes of these 236 DB/DEGs revealed a moderate positive correlation between Rad53 binding change and gene expression change, with a Spearman r = 0.5918 (Figure 5c, left panel). Among this group, 51 out of 54 genes with decreased Rad53 signal were down-regulated in mRNA levels, whereas genes with increased Rad53 signals partitioned into both up-regulation and down-regulation (108 and 74, respectively). Further break down of the 236 DB/DEGs group by co-expression clusters revealed that genes in clusters 1 and 7 exhibited the most significant positive correlation between Rad53 binding and gene expression changes (Figure 5c, r = 0.5697 ($p < 0.000001$) and r = 0.6979 ($p < 0.000037$), respectively). Thus, specific subsets of DEGs in the shift from G1→ HU exhibited correlations between a change in gene expression and Rad53 promoter binding.

Checkpoint mutants cause down-regulation of gene expression near promiscuously active late origins

We further inspected the localization of Rad53 in a subset of DEG clusters from the HU45 (*mrc1Δ* vs *WT*) comparison (Figure 6a) and the HU45 (*rad53*^{K227A} vs *WT*) comparison (Figure 6 – figure supplement 1a). In these analyses, we noticed a characteristic pattern, in which down-regulated genes tended to have a strong Rad53 signal not only upstream of the TSS, but a broad signal within gene bodies (Figure 6b and – figure supplement 1b). This pattern was prominent in the *mrc1Δ* mutant in HU45 and further intensified in HU90. The gene body localization was also found more transiently in HU45 sample from *rad53*^{K227A} cells. This signal pattern was not as prevalent in the *WT* HU45 and HU90 samples. Since Rad53 is also recruited to active origins and moves with the replication fork, we suspected that these gene body signals in the checkpoint mutants were caused by the promiscuous activation of near-by origins that are normally inactive in *WT*, creating conflicts between DNA replication and gene transcription. The transient nature of the Rad53 localization at gene bodies in this group of genes in the *rad53*^{K227A} mutant is also consistent with the transient signal pattern at origins (Figure 2 – figure supplement 3c). Thus, we investigated the relationship between these genes and their closest replication origins.

The distance from the TSS of each gene to the nearest replication origins, the relative orientation of gene transcription to the origin (head-on or co-directional) and the origin type (early, late or inactive; see Definition of the origin-types in Materials and methods) was determined and presented in the same order as in the heatmaps of DEG clusters shown in Figure 6b (Figure 6c). Overall, most of the down regulated genes in cluster 1 of this group were situated very close to active origins (< 2 kb between origin center and TSS, light purple marks and <1 kb, dark purple marks). Interestingly, the pattern of marks for origin to TSS distance largely mirrored the patten of the Rad53 ChIP signal within the gene bodies (Figure 6, b and c). This correlation pattern was not found in the *WT* ChIP heatmaps.

To explore the functional relationship between replication origins and genes, we summarized the ratio of up- and down-regulated DEGs from the HU45 (*mrc1Δ* vs *WT*) comparison in terms of the category of their relation to the closest origins (Figure 6d). In the first category, we parsed this DEG group according to the range of distance between TSS and closest origins (Figure 6d, left panels). Within this DEG group, genes situated 5 kb or more away from the closest active

origins were similarly distributed between up regulation and down regulation of gene expression. However, for those genes that are closer to an active origin (<5 kb), the bias toward down regulated genes increased. For those genes situated less than 1 kb away from active origins, more than 80% were down-regulated. In the second category, we grouped the DEGs according to the type origin the TSS was closest to. The DEGs that are more than 5 kb away from any annotated origins were labelled "none" in origin type (Figure 6d, middle panels) and similarly distributed between up and down regulation as expected from the above analysis. However, more down-regulated genes were found when the nearby origins were active (Figure 6d, origin type late or early). The bias was stronger for genes that were close to late origins, which become active in HU when Mrc1 was absent (86 % and 71 % down-regulated when genes were close to late and early origins, respectively, Fisher's exact test $p = 0.012$). Because late origins and intermediate early origins were more active in the *mrc1Δ* mutant, it is possible that nearby gene expression was negatively affected by active DNA synthesis. In the third category, we examined the effect of relative gene-origin orientation. We found that the bias toward the down regulation was stronger when the nearby origin (<5 kb away) was in a head-on (HO) orientation than in a co-directional (CD) orientation towards the gene (86 % and 67 % down-regulated for HO and CD sets, respectively, Fisher's exact test $p = 0.0019$) (Figure 6d, right panels). Thus, untimely activation of DNA replication origins in the checkpoint mutants affects gene expression concomitant with Rad53 binding to gene bodies.

Rad53 binding changes coincide with the changes in gene expression for targets of cell cycle regulators SBF and MBF

Two clusters from the gene co-expression analysis of DEGs in the *WT*(G1→HU45) comparison showed a significant correlation between Rad53 binding and gene expression (Figure 5c and d, clusters 1 and 7). These two clusters contain genes that encode targets of SBF and MBF, key transcription factor complexes comprised of a shared regulatory subunit, Swi6 and the DNA-binding subunits Swi4 and Mbp1, respectively (Breeden, 2003). Their target genes include multiple G1- and S-phase cyclin genes, such as *PCL1*, *CLN1*, *CLN2*, *CLB5*, *CLB6*. Evidence suggests that SBF and MBF are directly regulated by Rad53 kinase and Rad53 may regulate expression of targets of Msn4, Swi6, Swi4, and Mbp1 through Dun1-independent mechanisms (Jaehnig et al., 2013; Oliveira et al., 2012; Sidorova and Breeden, 2003; Travesa et al., 2012). Thus, we analyzed the annotated targets of these transcription factors compiled in the *Saccharomyces* Genome Database (SGD; https://www.yeastgenome.org). Among the 81 genes that are candidate targets for both Swi4 and Swi6, 36 genes were found in the 236 DB/DEGs (Figures 3b and 5c) with an increase of frequency from 1.18 % to 15.25 % ($p < 1E-15$). Scatter plot comparisons of Rad53 binding and gene expression changes of these 36 genes show a clear positive correlation (Figure 7a, SBF top panel). Comparing with data from the checkpoint mutant samples, we found that most of these SBF target genes showed a similar profile of differential expression, from G1 to HU, in the *rad9Δ* mutant to that in *WT* (Figure 7b). However, in the *mrc1Δ* and *rad53*^{K227A} mutants, a subgroup of genes, for example *RNR1*, *SRL1* and *YMR279C*, exhibited different levels of change from that in *WT* (Figure 7b). We also found significant enrichment for targets of MBF (targets for both Mbp1 and Swi6 in SGD annotation) and transcription factor Msn4 among the 236 DB/DEGs group, as well as positive correlations between Rad53 promoter binding and gene expression changes in these transcription factor

targets (Figure 7a). Noticeably, there are 19 genes in these TF target group being both targets of SBF and MBF, and 12 out of 22 Msn4 targets that are also SBF targets.

Many of the genes with decreased Rad53 binding at the promoters are mating response genes (Figures 3b and 3c, bottom panels). Therefore, the targets of Ste12, a key transcription factor activated by MAPK signaling to regulate genes involved in mating or pseudohyphal/invasive growth pathways were investigated. Of 183 potential targets of Ste12 annotated in SGD, 34 were in the 236 DB/DEGs group (Figures 5c and 7a). All the Ste12 targets that have decreased Rad53 binding were down regulated as cells entered S-phase. Moreover, 20 out of the 34 Ste12 targets in the Top DB group showed increased Rad53 binding in HU and 11 of these 20 genes were also targets of SBF. Thus, regulation by SBF may be responsible for the correlation between increased Rad53 binding at the promoter and up-regulation of these target genes.

SBF is a key factor for recruitment of Rad53 to the promoters of its target genes under replication stress condition

To determine the contribution of various transcription regulators in recruitment of Rad53 to gene promoters, we performed Rad53 ChIP-seq experiments for *WT*, *ixr1Δ*, *swi4Δ* and *swi6Δ* mutants (experiment TF). The *ixr1Δ* mutant was also examined because a previous investigation found that Ixr1 binds to the *RNR1* promoter upon genotoxic stress and mediates Dun1-independent *RNR1* gene regulation that requires Rad53 (Tsaponina et al., 2011). In the scatter plot of the Rad53 signal upstream of TSSs in G1 versus HU45 from the *WT* dataset, SBF targets in the Top DB (Figure 8a, orange/red diamonds) showed substantial deviation from the general trend (blue dots). In *swi4Δ* and *swi6Δ* mutants, the signal for all of these SBF targets collapsed towards the general trend (purple and light olive dots, *swi6Δ* and *swi4Δ*, respectively), suggesting that Rad53 signal changes at these genes depended on SBF. Analysis of Z-score distribution for Rad53 DB residual (G1→HU45) also showed substantial deviation of SBF target genes from the rest of the genes in *WT* (Figure 8b), while in the *swi4Δ* and *swi6Δ* mutants, the deviation of the SBF targets was closer to other genes. Coverage tracks for Rad53 ChIP-seq signals showed that in the SBF mutants Rad53 binding was completely eliminated from the *TOS6* (target of SBF 6) promoter while for *PCL1* and *YOX1,* both targets of SBF, Rad53 binding did not increase in HU, in contrast to the pattern in *WT* (Figure 8c). Thus, SBF is important for the recruitment of Rad53 to the promoters of SBF target genes under replication stress. Interestingly, at the promoter of *RNR3*, the paralog of *RNR1*, Rad53 binding in the SBF mutants was low, even though *RNR3* is known to be target of Rfx1 and not known as target of SBF or MBF. Thus, it is possible that, in addition to Rfx1, SBF also plays a role in regulation of *RNR3* in response to replication stress.

In the *ixr1Δ* mutant, the Z-score distribution of Rad53 DB residual (G1→HU45) showed a deviation similar to the level in *WT* (Figure 8b), and the Rad53 ChIP-seq signal for the majority of these SBF targets remained deviated from the general trend in the scatter plot. However, one clear exception was the *RNR1* gene, indicated in the close-up plots (Figure 8a, lower panels), whose position collapsed in all three mutants, consistent with *RNR1* being a target of Ixr1, SBF and MBF (Bruin et al., 2006; Tsaponina et al., 2011).

Discussion

Previous studies have implicated Rad53 kinase in regulation of gene expression through direct interaction with various transcription regulators (Jaehnig et al., 2013; Oliveira et al., 2012; Sidorova and Breeden, 2003; Travesa et al., 2012). Unexpectedly, we found that Rad53 bound to about 20% of the gene promoters in the yeast genome. These genes encode proteins with diverse functions, including various aspects of cell cycle, metabolism, protein modification, ion transport, cell wall organization and cell growth. There is a general trend of increasing Rad53 level during the G1 to S phase transition in the presence of HU (Figures 2a and 3a). Remarkably, Rad53 binding at promoters for genes such as *RNR1*, *RNR3* and *TOS6* increases substantially beyond the general trend (Figures 2c and 3c). In contrast, Rad53 binding decreased at promoters of genes involved in response to mating pheromone as cells exited from α-factor induced G1 arrest into the cell division cycle. The prevalent and dynamic changes in Rad53 promoter-bound levels in cells replicating in HU did not necessarily depend on checkpoint signaling activated by HU, for example, at genes like *PCL1* and *YOX1*. But in some cases, such as *RNR1*, the increase in Rad53 levels was reduced in checkpoint mutants (Figure 2 – figure supplement 4). Furthermore, the Mrc1 checkpoint mediator, Mec1 sensor kinase and kinase activity of Rad53 itself are not absolutely required for the recruitment of Rad53 to gene promoters (Figure 1b and Figure 4 – figure supplement 1). The binding of Rad53 to numerous promoters in the yeast genome suggests a previously unappreciated level of transcription regulation that is coordinated with the many cellular processes, such as normal DNA replication, and induced cellular stresses to which Rad53 responds.

The conditions employed in this study, cell cycle entry in the presence of hydroxyurea, may determine the nature of the genes that display dynamic binding of Rad53 to gene promoters. It is known that Rad53 phosphorylates transcription factors such as the SBF and MBF subunit Swi6 and the MBF co-repressor Nrm1 (Oliveira et al., 2012; Sidorova and Breeden, 2003; Travesa et al., 2012) and that Irx1controls transcription of *RNR1* (Tsaponina et al., 2011). Removal of Swi4, Swi6 or Ixr1 reduced, and in some cases eliminated Rad53 binding to promoters of genes controlled by these transcription factors. We also found Rad53 bound to the *NRM1* promoter, which is also in the Top DB group, suggesting an additional regulation of cell cycle-dependent transcription control by Rad53. Rad53 also bound to promoters of genes encoding histones and all histone genes were upregulated DEGs in the HU45 (*rad53*^{K227A} vs *WT*) comparison (Figure 6 – figure supplement 1), suggesting that, in addition to its known role in histone degradation (Gunjan and Verreault, 2003), Rad53 may control histone level through gene expression. This is consistent with previous findings that Rad53 targets Yta7 (Smolka et al., 2006), which interacts with FACT to regulate histone gene expression and inhibits Spt21^{NPAT}-regulated histone genes expression (Bruhn et al., 2020; Gradolatto et al., 2008). In the absence of Rad53 protein, histone levels become elevated, causing global effects on gene expression (Bruhn et al., 2020; Tsaponina et al., 2011).

Our data is consistent with the possibility that the Rad53 protein contributes to the transcriptional regulation as a structural component by binding directly to promoters or transcriptions factors bound to these promoters, as previously suggested for several MAP kinases (Alepuz et al., 2001; Kim et al., 2008; Sanz et al., 2018). Like the stress induced kinase Hog1, Rad53 binding to promoters may be dynamic in other stress conditions, which is under investigation. A major unanswered question is how Rad53 binds to so many diverse promoter sites. We suggest that it

may bind DNA directly or to a common factor that is present at the promoters of Rad53 bound genes. Alternatively, certain chromatin features common to these promoters may facilitate Rad53 recruitment. It remains possible that, in addition to transcriptional regulation, Rad53 may be recruited to promoter region preemptively to ensure integrity of vulnerable chromatin associated with active transcription. Pre-targeting repair complexes to open chromatin where they are poised for lesion recognition and repair has been reported in human cells (Bacolla et al., 2020).

In cells, the same DNA template is used for both replication and transcription, potentially creating conflicts between replication and transcription that can lead to detrimental effects on genome stability and cell viability (Hamperl and Cimprich, 2016). Thus, it is important that cells employ mechanisms to avoid, tolerate and resolve such conflicts. It is known that late replicating genes are tethered to the nuclear pore complexes in the nuclear periphery and checkpoint signaling, including Rad53 kinase, is required for preventing topological impediments for replication fork progression (Bermejo et al., 2011; Hamperl and Cimprich, 2016). Moreover, during normal replication, Mec1 may locally activate Rad53 to deal with difficult to replicate loci or regions of replication-transcription conflict without triggering full blown checkpoint activation (Bastos de Oliveira et al., 2015).

Eukaryotic cells initiate DNA synthesis in a temporally controlled manner from multiple replication origins to ensure efficient duplication of the genome (Bell and Labib, 2016; Renard-Guillet et al., 2014). One of the main consequences of checkpoint activation is inhibition of late origin firing (Tercero et al., 2003). However, in the checkpoint mutants, these late origins become active and we found that Rad53 was recruited to the body of origin proximal genes. Concomitantly, gene expression of these genes was reduced, perhaps mediated by recruitment of Rad53. While checkpoint signaling pathways are known to regulate gene expression, it is possible that untimely activation of the late origins results in a replication-transcription conflict and contribute to down-regulation of genes in these checkpoint mutants. We suggest that the normal temporal order of replication of genes in the genome throughout S-phase, and possibly the order of transcription of genes, have evolved to prevent conflicts between replication and transcription, which is particularly important in a gene dense genome such as *S. cerevisiae*.

Acknowledgements

This research was supported by NIH grants R01GM45436 and R01LM012736 and a gift from the Goldring Family Foundation. The Cold Spring Harbor Laboratory Cancer Center supported core research resources (P30-CA045508). RKK was supported by Uehara Memorial Foundation Postdoctoral Fellowship.

Materials and methods

Yeast strains and methods

Yeast strains generated in this study were derived from W303-1a (*MATa ade2-1 can1-100 his3-11,15 leu2-3,112 trp1-1 ura3-1*) and are described in Supplemental Table 1. All the yeast strains used for the whole-genome DNA replication profile analyses have a copy of the BrdU-Inc

cassette inserted into the URA3 locus (Viggiani and Aparicio, 2006). For G1 arrest of *bar1Δ* strains, exponentially growing yeast cells (~10^7 cell/mL) in YPD were synchronized in G1 with 25 ng/mL of α-factor for 150 min at 30°C. For G1 arrest of *BAR1* strains, exponentially growing cells were grown in normal YPD, then transferred into YPD (pH3.9), grown to ~10^7 cell/mL, and then synchronized in G1 with three doses of α-factor at 2 µg/mL at 0-, 50-, and 100-min time point at 30°C. Cells were collected at 150 min for release. To release from G1 arrest, cells were collected by filtration and promptly washed twice on the filter using one culture volume of H_2O and then resuspended into YPD medium containing 0.2 mg/mL pronase E (Sigma).

Protein sample preparation and immunoblot analysis

TCA extraction of yeast proteins was as described previously (Sheu et al., 2014). For immunoblot analysis, protein samples were fractionated by SDS-PAGE and transferred to a nitrocellulose membrane. Immunoblot analyses for Orc6 (SB49), Rad53 (ab104232, Abcam) , γ-H2A (ab15083, Abcam) and Sml1 (**AS10 847, Agrisera**) were performed as described (Sheu et al., 2016, 2014).

Isolation and preparation of DNA for whole-genome replication profile analysis

Modified protocol based on previously described (Sheu et al., 2016, 2014). Briefly, yeast cells were synchronized in G1 with α-factor and released into medium containing 0.2 mg/mL pronase E, 0.5 mM 5-ethynyl-2′ -deoxyuridine (EdU) with or without addition of 200 mM HU as indicated in the main text. At the indicated time point, cells were collected for preparation of genomic DNA. The genomic DNA were fragmented, biotinylated, and then purified. Libraries for Illumina sequencing were constructed using TruSeq ChIP Library Preparation Kit (Illumina). Libraries were pooled and submitted for 50 bp paired-end sequencing.

Sample preparation for Chromatin immunoprecipitation coupled to deep sequencing (ChIP-seq)

Chromatin immunoprecipitation (ChIP) was performed as described (Behrouzi et al., 2016) with modification. About 10^9 synchronized yeast cells were fixed with 1% formaldehyde for 15 min at room temperature (RT), then quenched with 130 mM glycine for 5 min at RT, harvested by centrifugation, washed twice with TBS (50 mM Tris.HCl pH 7.6, 150 mM NaCl), and flash frozen. Cell pellets were resuspended in 600 µL lysis buffer (50 mM HEPES-KOH pH 7.5, 150 mM NaCl, 1 mM EDTA, 1% Triton X-100, 0.1% Na-Deoxycholate, 0.1% SDS, 1 mM PMSF, protease inhibitor tablet (Roche)), and disrupted by bead beating using multi-tube vortex (Multi-Tube Vortexer, Baxter Scientific Products) for 12-15 cycles of 30 seconds vortex at maximum intensity. Cell extracts were collected and sonicated using Bioruptor (UCD-200, Diagenode) for 38 cycles of pulse for 30 seconds ”ON”, 30 seconds “OFF” at amplitude setting High (H). The extract was centrifuged for 5 min at 14,000 rpm. The soluble chromatin was used for IP.

Antibodies against Cdc45 (CS1485, this lab (Sheu and Stillman, 2006)), Rad53 (ab104232, Abcam) , γ-H2A (ab15083, Abcam) was preincubated with 1:1 mixture of washed Dynabeads Protein A and G (1002D and 1004D, Invitrogen) for more than 30 min at room temperature and washed twice with lysis buffer to remove unbound antibodies. For each immunoprecipitation, 80 µl antibody-coupled Dynabeads was added to soluble chromatin. Samples were incubated overnight at 4°C with rotation, after which the beads were collected on magnetic stands, and washed 3 times with 1 mL lysis buffer and once with 1 mL TE, and eluted with 250 µl preheated

buffer (50 mM Tris.HCl pH 8.0, 10 mM EDTA, 1% SDS) at 65°C for 15 min. Immunoprecipitated samples were incubated overnight at 65°C to reverse crosslink, and treated with 50 µg RNase A at 37°C for 1 hr. Then 5 µl proteinase K (Roche) in 20 mg/mL stock was added and incubation was continued at 55°C for 1 hr. Samples were purified using MinElute PCR purification kit (Qiagen). Libraries for Illumina sequencing were constructed using TruSeq ChIP Library Preparation Kit (IP-202-1012 and IP-202-1024, Illumina).

Sample preparation for RNA seq

About 2-3x10^8 flash-frozen yeast cells were resuspended in Trizol (cell pellet: Trizol = 1:10) and vortexed for 15 sec and incubated at 25ºC for 5 min. Subsequently, 200 µl chloroform was added per 1 mL of Trizol-cell suspension and samples were vortexed for 15 sec, incubated at room temperature for 5 min and centrifuged to recover the aqueous layer. The RNA in the aqueous layer were further purified and concentrated using PureLink Column (12183018A, Invitrogen). The RNA was eluted in 50 µL and store at -20ºC if not used immediately. Store at -80ºC for long term. Paired-end RNA-seq libraries were prepared using TruSeq stranded mRNA library preparation kit (20020594, Illumina).

Generation of coverage tracks using the Galaxy platform

For visualization of read coverage in the Integrated Genome Browser (Freese et al., 2016), the coverage tracks were generated using the Galaxy platform maintained by the Bioinformatics Shared Resource (BSR) of Cold Spring Harbor Lab. The paired-end reads from each library were trimmed to 31 bases and mapped to sacCer3 genome using Bowtie (Langmead, 2010). The coverage track of mapped reads was then generated using bamCoverage (Ramírez et al., 2014) with normalization to 1x genome.

Definition of the origin-types

Based on the BamCoverage output for EdU signal in *WT*, *rad53*^{K227A} and *mrc1Δ*, we categorized 829 origins listed in the oriDB database (Siow et al., 2012). We define the early origins as the one whose signal at the first time point is larger than 2. The late origins are extracted from the rest of the origins if the average signal value at the later time point is larger than 2 in *rad53*^{K227A} and *mrc1Δ* mutants. Among the 829 entries in oriDB, we defined 521 as active origins (with EdU signal in *WT* or checkpoint mutants *rad53*^{K227A} and *mrc1Δ*), in which 256 was categorized as early origins (with EdU signal in *WT*) and 265 as late origins (with signal in checkpoint mutants but not in *WT*). The remaining 308 entries do not have significant signal under our condition and were deemed inactive origins.

Computational analysis of sequence data

The sequenced reads were trimmed by cutadapt with an option of "nextseq-trim", then aligned by STAR (Dobin et al., 2013) in a paired-end mode to the sacCer3 genome masked at repetitive regions. The gene structure is referred from SGD reference genome annotation R64.1.1 as of Oct. 2018. For RNA-seq quantification analysis, the total counts of aligned reads were computed for each gene by applying "GeneCounts" mode. For ChIP-seq quantification analysis, the reads were mapped using the same pipeline. We also confirmed the mapped reads found in ChIP-seq data do not span a long range (the median span is from 169.5 to 329, 90% paired-end reads are aligned within less than 6000 bp window), suggesting that STAR spliced alignment do not affect the alignment results. Additionally, peak calling was done by MACS2 in a narrow

peak mode. Distribution of Rad53 ChIP-seq peaks was computed using ChIPpeakAnno (https://www.rdocumentation.org/packages/ChIPpeakAnno/versions/3.6.5/topics/assignChromosomeRegion).

The Gini indexes were calculated from Lorenz curves using Rad53 ChIP-Seq datasets and published ChIP-Seq data for Swi6 (SRX360900<https://www.ncbi.nlm.nih.gov/sra/SRX360900%5baccn%5d>: GSM1241092: swi6 DMSO illumina; Saccharomyces cerevisiae; ChIP-Seq), using DescTools (Andri Signorell et mult. al. (2021). DescTools: Tools for descriptive statistics. R package version 0.99.41, https://cran.r-project.org/package=DescTools).

Gene expression analysis

Differentially expressed genes (DEGs) and their p-values were computed for each pair of the cases by nbinomWaldTest after size factor normalization using DESeq2 (Love et al., 2014). Using the list of DEGs, GO and KEGG enrichment analyses were performed via Pathview library. ClusterProfiler was applied to visualize fold changes of DEGs in each KEGG pathway. Co-expression analysis of significant DEGs was further performed based on co-expression network constructed in CoCoCoNet (Lee et al., 2020). CoCoCoNet has established the co-expression matrix of Spearman's correlation ranking based on 2,690 samples downloaded from SRA database. We carried out clustering for the correlation matrix downloaded from CoCoCoNet (yeast_metaAggnet) by dynamicTreeCut in R (or hierarchical clustering) to obtain at most 10 clusters. The enrichment analysis for the gene set of each cluster was performed in the same way with RNA-seq analysis.

ChIP-seq signal normalization

For ChIP-seq signal normalization, two different methods were applied to different types of analysis. For ChIP-seq residual analysis, we used simple normalization. In this process, each case sample was compared with the corresponding control sample of DNA input to compute log2 fold changes within each 25 bp window reciprocally scaled by multiplying the total read counts of another sample. Then, the average of fold changes was computed for each duplicate. For ChIP-seq heatmap analysis, we employed the origin-aware normalization to account for the higher background around origin region as a result of DNA replication. In the origin-aware normalization, the same computation used in simple normalization, or log2 fold change with scaling by the total read count, is independently applied for the region proximal to the origins and others. For the heatmap presented in this paper, the origin-proximal region is defined as the region within 5,000 bp upstream and downstream.

Heatmap analyses at origins and TSS

After the average fold change computation and normalization from ChIP-seq signals, the signal strength is visualized around the target regions such as TSSs and replication origins are extracted using normalizeToMatrix function in EnrichedHeatmap (window size is 25 bp and average mode is w0). We ordered heatmaps to examine a different signal enrichment pattern for the characteristics of each origin or gene. For the heatmap row of each origin is ordered by the assigned replication timing for ChIP-seq signals around replication origins. The replication time for the origins are annotated with the replication timing data published previously (Yabuki et al., 2002). From the estimated replication time for each 1,000 bp window, we extracted the closest

window from the center of each replication origin and assigned it as the representative replication timing if their distance is no more than 5,000 bp. Early and late origins groups are categorized according to the definition of the origin-types using the replication profile data from this study. The final set of the replication origins used in the heatmap analysis are obtained after filtering out the replication origins overlapped with any of 238 hyper-ChIPable regions defined in the previous study (Teytelman et al., 2013). In total, 167 early and 231 late origins pass this filter and are used in the heatmaps analysis in this study. For heatmaps of the ChIP-seq signals around TSS, we ordered genes based on RNA-seq fold changes for all DEGs or per co-expression cluster of DEGs based on gene co-expression network constructed in CoCoCoNet (Lee et al., 2020).

ChIP-seq residual analysis

To detect the time-dependent increase or decrease of Rad53 binding signals, we first focused on the 500 bp window upstream from each TSS (defined as promoter region) and computed the sum of the fold change signals estimated for each 25-bp window scaled by the window size as an activity of Rad53 binding for each gene. The overall activity scores are varied for each time point probably because of the different Rad53 protein level or other batch-specific reasons. To adjust such sample specific differences for a fair comparison, a linear regression is applied for the activity scores of all genes between G1 and other time points HU45 and HU90 using lm function in R. Then we selected top genes showing the deviated signals from the overall tendency according to the absolute residual values between the actual and predicted values, excluding the genes with signal value lower than -0.075 after scaling the maximal signal to 1. Top 1,000 genes with the highest absolute residual values were selected from 2 independent experiments. The 435 DB genes identified in both experiments (435 Top DB overlap) were selected for further analysis.

Data Availability

All data supporting this work are available at public sites. Sequencing data is available at Dryad (https://doi.org/10.5061/dryad.tx95x69xv). Source data are provide with this paper (URL XXX).

Code Availability

R scripts for the co-expression analyses including clustering and enrichment analysis are available at https://github.com/carushi/yeast_coexp_analysis.

Figure legends

Figure 1. Rad53 is recruited to genomic loci other than replication origins in proliferating yeast cells

a, Coverage tracks of Rad53 ChIP-seq signals in *WT*, *sml1Δ*, *rad53Δsml1Δ* and *mec1Δ sml1Δ* for chromosome III. Asynchronous yeast cultures were processed for ChIP-seq analysis for distribution of Rad53 at genomic loci. The results from two independent experiments are presented. Experiment 1 compares only *sml1Δ*, *rad53Δsml1Δ*. **b,** Heatmaps and average signals of Rad53 across 2 kb intervals centered on transcription start sites (TSSs) for proliferating *WT*,

sml1Δ, *rad53Δsml1Δ*, and *mec1Δ sml1Δ* cells. **c**, Heatmaps of ChIP-seq signals across 30 kb intervals centered on all origins annotated in OriDB database (Siow et al., 2012).

Figure 2. Rad53 is recruited to TSS and the binding changes with the cell cycle stage
Cells were synchronized in G1 phase and released into YPD containing 0.2 M HU for 45 and 90 min (HU45 and HU90, respectively). **a**, Heatmaps and average signals of Rad53 and γ-H2A ChIP-seq signals across 2 kb intervals centered on TSSs for *WT* cells at stages of G1, HU45 and HU90. **b,** Distribution of aggregated peak numbers around TSS using merged Rad53 ChIP-seq peaks from all three stages (G1, HU45 and HU90)Pie charts showing the distribution of Rad53 ChIP-seq peaks in relation to gene features. **c,** Rad53 ChIP-seq profiles near *RNR1*, *PCL1* and *TOS6* genes in proliferating *WT*, *sml1Δ*, *rad53Δ sml1Δ* and *mec1Δ sml1Δ* cells, and *WT* cells at stages of G1, HU45 and HU90. **d,** Lorenz curves for ChIP-seq read counts of Swi6 and Rad53 mapped to gene promoters showing inequality for promoter binding.

Figure 2 – figure supplement 1. Relative level of Rad53 protein changes in cells
a, Immunoblots monitoring protein status for Rad53, Orc6, γ-H2A and Sml1 during checkpoint activation from G1 to HU45 and HU90. **b,** Comparison of Rad53 protein level in G1 extracts from *WT*, *rad53*^{K227A}, *mrc1Δ* and *rad9Δ* cells. Blots for Orc6, γ-H2A and Sml1 are included for reference. **c,** Comparison of Rad53 protein level in HU90 extracts from *WT*, *rad53*^{K227A}, *mrc1Δ* and *rad9Δ* cells. 14 % SDS-PAGE was used for the Rad53 titration blot to allow collapsing of all phosphorylated forms into a single band. Two-fold dilutions of the samples are loaded.

Figure 2 – figure supplement 2. Comparison of ChIP-seq signals of γ-H2A and Rad53 with and without sequences found enriched promiscuously in previous studies
Heatmaps across 2 kb intervals centered on TSSs using ChIP-Seq data with antibodies against γ-H2A (**a** and **b**) or Rad53 (**c-e**). **a** and **c,** The complete datasets, **b** and **d**, the datasets following removal of the hyper-ChIPable regions and **e,** the signal data for genes only at the hyper-ChIPable regions observed by Teytelman et al. and Park et al. Note the pattern of Rad53 localization in **e** is both upstream and downstream of the TSSs, unlike that found for Rad53 ChIP-Seq surrounding TSSs in **c** and **d**. **f**, KEGG enrichment analysis for the 296 genes associated with hyper-ChIPable regions shows mostly tRNA and snoRNA genes.

Figure 2 – figure supplement 3. Heatmaps of ChIP-seq signal across 30 kb centered on all active origins
WT, *rad53*^{K227A} and *mrc1Δ* mutant cells at stages of G1, HU45 and HU90 were collected and processed for ChIP-seq analysis. **a, b, and c,** Heatmaps of ChIP-seq signal of Cdc45, γ-H2A and Rad53, respectively, across 30 kb intervals centered on all active origins (see Definition of the origin-types in methods section). Origins are ordered according to the associated replication timing data reported in previous study (Yabuki et al., 2002).

Figure 2 – figure supplement 4. Rad53 ChIP-seq profiles near *RNR1*, *PCL1* and *TOS6* genes in at stages of G1, HU45 and HU90.
Coverage tracks of Rad53 ChIP-seq signals from *WT*, *rad53*^{K227A} and *mrc1Δ* mutant datasets at stages of G1, HU45 and HU90.

Figure 3. Identification of genes with Rad53 binding changes at the promoters

a, Scatter plots compare the signals in G1 (x-axis) and HU45 (y-axis) at 500 bp intervals upstream of TSSs for all genes in *WT* datasets from two independent experiments, TF and CP. Orange dots indicated the 1000 genes with highest binding changes (Top 1000 DB) and satisfying the filter of minimal signal of -0.075 (Maximal = 1). The Venn diagram to the right illustrates the identification of 435 genes that are found in both experiments (435 Top DB overlap). **b**, Binding changes (y-axis: residuals from analysis of experiment TF) for 435 Top DB overlap. **c,** Examples of coverage tracks for selected genes show Rad53 signal changes at the indicated gene promoters from G1 to HU45 and HU90.

Figure 4. **Gene expression changes in *WT* and checkpoint mutants under stress and the tendency of higher Rad53 binding at promoter of genes with significant differential expression**

WT, *rad9Δ*, *rad53*^{K227A} and *mrc1Δ* cells were synchronized in G1-phase and released into YPD containing 0.2 M HU. Cells at stages of G1, HU45 and HU90 were collected and processed for RNA-seq analysis. **a,** Rank data analysis of RNA-seq samples. **b**, Bar graph summarizing on the x-axis the number of genes that show statistically significant differential expression (DEGs). The types of pairwise comparison are indicated to the right. Blue bars, down-regulated DEGs. Orange bars, up-regulated DEGs. **c**, Average Rad53 ChIP-seq signal across 2 kb intervals centered on at TSS for statistically significant DEGs (red) and the insignificant (cyan). Left panel shows the result of DEGs from comparison of G1 and HU45 datasets of *WT* (DEGs: *WT*(G1→HU45)) and right panel shows DEGs from comparison of G1 and HU90 datasets (DEGs: *WT*(G1→HU90))

Figure 4 – figure supplement 1. Average Rad53 ChIP-seq signal and heatmaps of signal across 2 kb intervals centered on TSS for stage-dependent differentially expressed genes (DEGs)

a, Rad53 ChIP-seq signal in *WT*, *rad53*^{K227A} and *mrc1Δ* mutant cells at stages G1, HU45 and HU90 for DEGs from *WT*(G1→HU45) (upper panel) and from *WT*(G1→HU90) (lower panel; the ordering of datasets is the same as in upper panel). **b and c,** Rad53 ChIP-seq signal in DEGs from *rad53*^{K227A}(G1→HU45) and *mrc1*Δ(G1→HU45), respectively. The ordering of datasets is the same as in **a**. Genes in each heatmap group are arranged in descending order according to the differential expression level (i.e., log2 fold change (log2FC)). The graphs plotted on top of the heatmaps show the average ChIP-seq signals for significant (red) and for the insignificant (cyan) from comparisons indicated at the left of panels.

Figure 5. **Correlation between differential binding of Rad53 at promoter and differential gene expression**

a, Co-expression cluster matrix for significant DEGs in *WT*(G1→HU45). Cluster (C): color codes for DEG clusters. Gene(G): level of differential expression in log2FC. **b**, Heatmaps of Rad53 ChIP-seq signal across 2 kb intervals centered on TSS parsed by the DEG clusters in **a**. Genes within each cluster are arranged in descending order according to the differential expression level (i.e., log2FC). **c**, Scatter plots of Rad53 binding changes at the promoter against expression changes for the 236 significant DEGs in the 435 Top DB overlap group (leftmost panel) and subgroups in clusters 1, 2, 4 and 7. Spearman correlation r is indicated on top of each plot (****, $p < 0.0001$; *, $p < 0.05$). N, number of genes in the group analyzed. **d**, Result of Fisher's exact test for association between binding changes (DB) and expression changes (DE)

for groups presented in **c**. ****, $p < 0.0001$; **, $p < 0.01$; ns, not significant. Examples of genes in the cluster are shown below the plot.

Figure 6. Origin-proximal DEGs are biased towards down-regulation in the *mrc1Δ* mutant.
DEGs from HU45 (*mrc1Δ* vs *WT*) comparison were analyzed. **a,** Co-expression cluster matrix for significant DEGs. Cluster (C): color codes for DEG clusters. Gene(G): level of differential expression in log2FC. **b**, Heatmaps of Rad53 ChIP-seq signal across 2 kb intervals centered on TSS parsed by the DEG clusters in **a**. ChIP-seq signal in *WT*, *rad53*^{K227A} and *mrc1Δ* mutant cells at stages G1, HU45 and HU90 are shown. **c**, Summary of gene-origin relation for DEGs co-expression clusters. Distance between each TSS and its nearest origin center is indicated in pink gradient as well as light purple (<2 kb) and dark purple (<1 kb). Relative TSS-origin orientation and origin type are indicated. **d**, Stacked bar charts presenting number (top panels) and proportion (bottom panels) of down- and up-regulated DEGs as categorized by i) TSS to origin distance (left panels), ii) closest origin type within 5 kb of TSS (middle panels; none: no origins within 5 kb of TSS) and iii) origin-gene orientation (right panels; CD: co-directional; HO: head-on).

Figure 6 – figure supplement 1. Origin-proximal DEGs are biased towards down-regulation in the *rad53*^{K227A} mutant.
a. Co-expression cluster matrix for significant DEGs from HU45 (*rad53*^{K227A} vs *WT*) comparison. Cluster (C): color codes for DEG clusters. Gene(G): level of differential expression in log2FC. **b,** Heatmaps of Rad53 ChIP-seq signal across 2 kb intervals centered on TSS for DEG clusters in **a**. ChIP-seq signal in *WT*, *rad53*^{K227A} and *mrc1Δ* mutant cells at stages G1, HU45 and HU90 are shown. **c,** Summary of gene-origin relation for DEGs co-expression clusters from HU45 (*rad53*^{K227A} vs *WT*). Distance between each TSS and its nearest origin center is indicated in pink gradient as well as light purple (<2 kb) and dark purple (<1 kb). Relative TSS-origin orientation and origin type are indicated.

Figure 7. Differential binding of Rad53 at promoters and differential expression of target genes of SBF, MBF, Msn4 and Ste12
a, Top panels: scatter plots of binding changes (DB residual) and expression changes (log2 FC) for targets of indicated transcription regulators that are in the 236 DB/DEGs group. Spearman correlation r is shown under each plot (****, $p < 0.0001$; ***, $p < 0.001$; **, $p < 0.01$). N, number of genes in the group analyzed. Result of Fisher's exact test for enrichment of each group of transcription regulator targets in the 236 DB/DEGs is also indicated below. **b**, Profiles of differential expression in column graphs for each of the 36 SBF targets in the 236 DB/DEGs. Color coded columns showing expression change (Log2 FC (G1→HU45) and Log2 FC (G1→HU90)) extracted from *WT*, *rad53*^{K227A}, *mrc1Δ* and *rad9Δ* datasets.

Figure 8. SBF plays a major role in the localization of Rad53 to the promoters of its target genes under replication stress
a, Top panels: Scatter plots compare Rad53 ChIP-seq signals in G1 (x-axis) and HU45 (y-axis) at 500 bp intervals upstream of TSSs for all genes in *WT*, *ixr1Δ*, *swi4Δ* and *swi6Δ* mutants. Signals for SBF targets found in the 435 Top DB overlap are shown as orange or red diamond (*RNR1* in red diamond). Signals for the rest of genes are shown as dots in color blue (*WT*),

green (*ixr1Δ*), purple (*swi6Δ*) and light olive (*swi4Δ*). Bottom panels: Close-up for specific area from above panels. **b**, Box plots showing Z-score distribution for DB residuals (G1→HU45) for genes that are annotated as targets for both Swi4 and Swi6 (SBF targets) and genes that are otherwise (Others) in *WT*, *ixr1Δ*, *swi4Δ* and *swi6Δ* mutants (*p*-value by Wilcoxon rank sum test: *WT*, 2.2e-16; *ixr1Δ*, 3.174e-12; *swi4Δ*, 0.001608; *swi6Δ*, 0.002857). **c**, Coverage tracks showing distribution of Rad53 ChIP-seq signal near selected Top DB genes in *WT*, *ixr1Δ*, *swi4Δ* and *swi6Δ* mutants at stages of G1, HU45 and HU90.

References

Alepuz PM, Jovanovic A, Reiser V, Ammerer G. 2001. Stress-Induced MAP Kinase Hog1 Is Part of Transcription Activation Complexes. *Mol Cell* **7**:767–777. doi:10.1016/s1097-2765(01)00221-0

Bacolla A, Sengupta S, Ye Z, Yang C, Mitra J, De-Paula RB, Hegde ML, Ahmed Z, Mort M, Cooper DN, Mitra S, Tainer JA. 2020. Heritable pattern of oxidized DNA base repair coincides with pre-targeting of repair complexes to open chromatin. *Nucleic Acids Res* **49**:gkaa1120. doi:10.1093/nar/gkaa1120

Bastos de Oliveira FM, Kim D, Cussiol JR, Das J, Jeong MC, Doerfler L, Schmidt KH, Yu H, Smolka MB. 2015. Phosphoproteomics Reveals Distinct Modes of Mec1/ATR Signaling during DNA Replication. *Mol Cell* **57**:1124–1132. doi:10.1016/j.molcel.2015.01.043

Behrouzi R, Lu C, Currie M, Jih G, Iglesias N, Moazed D. 2016. Heterochromatin assembly by interrupted Sir3 bridges across neighboring nucleosomes. *Elife* **5**:e17556. doi:10.7554/elife.17556

Bell SP, Labib K. 2016. Chromosome Duplication in Saccharomyces cerevisiae. *Genetics* **203**:1027–1067. doi:10.1534/genetics.115.186452

Bermejo R, Capra T, Jossen R, Colosio A, Frattini C, Carotenuto W, Cocito A, Doksani Y, Klein H, Gómez-González B, Aguilera A, Katou Y, Shirahige K, Foiani M. 2011. The Replication Checkpoint Protects Fork Stability by Releasing Transcribed Genes from Nuclear Pores. *Cell* **146**:233–246. doi:10.1016/j.cell.2011.06.033

Breeden LL. 2003. Periodic Transcription: A Cycle within a Cycle. *Curr Biol* **13**:R31–R38. doi:10.1016/s0960-9822(02)01386-6

Bruhn C, Ajazi A, Ferrari E, Lanz MC, Batrin R, Choudhary R, Walvekar A, Laxman S, Longhese MP, Fabre E, Smolka MB, Foiani M. 2020. The Rad53CHK1/CHK2-Spt21NPAT and Tel1ATM axes couple glucose tolerance to histone dosage and subtelomeric silencing. *Nat Commun* **11**:4154. doi:10.1038/s41467-020-17961-4

Bruin RAM de, Kalashnikova TI, Chahwan C, McDonald WH, Wohlschlegel J, Yates J, Russell P, Wittenberg C. 2006. Constraining G1-Specific Transcription to Late G1 Phase: The MBF-Associated Corepressor Nrm1 Acts via Negative Feedback. *Mol Cell* **23**:483–496. doi:10.1016/j.molcel.2006.06.025

Callegari AJ, Kelly TJ. 2006. UV irradiation induces a postreplication DNA damage checkpoint. *Proc National Acad Sci* **103**:15877–15882. doi:10.1073/pnas.0607343103

Can G, Kauerhof AC, Macak D, Zegerman P. 2018. Helicase Subunit Cdc45 Targets the Checkpoint Kinase Rad53 to Both Replication Initiation and Elongation Complexes after Fork Stalling. *Mol Cell* **73**. doi:10.1016/j.molcel.2018.11.025

Desany BA, Alcasabas AA, Bachant JB, Elledge SJ. 1998. Recovery from DNA replicational stress is the essential function of the S-phase checkpoint pathway. *Gene Dev* **12**:1–15. doi:10.1101/gad.12.18.2956

Dobin A, Davis CA, Schlesinger F, Drenkow J, Zaleski C, Jha S, Batut P, Chaisson M, Gingeras TR. 2013. STAR: ultrafast universal RNA-seq aligner. *Bioinformatics* **29**:15–21. doi:10.1093/bioinformatics/bts635

Dohrmann PR, Sclafani RA. 2006. Novel role for checkpoint Rad53 protein kinase in the initiation of chromosomal DNA replication in Saccharomyces cerevisiae. *Genetics* **174**:87–99. doi:10.1534/genetics.106.060236

Forey R, Poveda A, Sharma S, Barthe A, Padioleau I, Renard C, Lambert R, Skrzypczak M, Ginalski K, Lengronne A, Chabes A, Pardo B, Pasero P. 2020. Mec1 Is Activated at the Onset of Normal S Phase by Low-dNTP Pools Impeding DNA Replication. *Molecular Cell*. doi:10.1016/j.molcel.2020.02.021

Freese NH, Norris DC, Loraine AE. 2016. Integrated genome browser: visual analytics platform for genomics. *Bioinformatics* **32**:2089–2095. doi:10.1093/bioinformatics/btw069

Gradolatto A, Rogers RS, Lavender H, Taverna SD, Allis CD, Aitchison JD, Tackett AJ. 2008. Saccharomyces cerevisiae Yta7 Regulates Histone Gene Expression. *Genetics* **179**:291–304. doi:10.1534/genetics.107.086520

Gunjan A, Verreault A. 2003. A Rad53 kinase-dependent surveillance mechanism that regulates histone protein levels in S. cerevisiae. *Cell* **115**:537–549. doi:10.1016/s0092-8674(03)00896-1

Hamperl S, Cimprich KA. 2016. Conflict Resolution in the Genome: How Transcription and Replication Make It Work. *Cell* **167**:1455–1467. doi:10.1016/j.cell.2016.09.053

Hoch NC, Chen ESW, Buckland R, Wang S-C, Fazio A, Hammet A, Pellicioli A, Chabes A, Tsai M-D, Heierhorst J. 2013. Molecular basis of the essential s phase function of the rad53

checkpoint kinase. *Molecular and Cellular Biology* **33**:3202–3213. doi:10.1128/mcb.00474-13

Holzen TM, Sclafani RA. 2010. Genetic interaction of RAD53 protein kinase with histones is important for DNA replication. *Cell Cycle* **9**:4735–4747. doi:10.4161/cc.9.23.14091

Huang M, Zhou Z, Elledge SJ. 1998. The DNA Replication and Damage Checkpoint Pathways Induce Transcription by Inhibition of the Crt1 Repressor. *Cell* **94**:595–605. doi:10.1016/s0092-8674(00)81601-3

Jaehnig EJ, Kuo D, Hombauer H, Ideker TG, Kolodner RD. 2013. Checkpoint kinases regulate a global network of transcription factors in response to DNA damage. *Cell reports* **4**:174–188. doi:10.1016/j.celrep.2013.05.041

Kim K-Y, Truman AW, Levin DE. 2008. Yeast Mpk1 Mitogen-Activated Protein Kinase Activates Transcription through Swi4/Swi6 by a Noncatalytic Mechanism That Requires Upstream Signal ▿ †. *Mol Cell Biol* **28**:2579–2589. doi:10.1128/mcb.01795-07

Langmead B. 2010. Aligning Short Sequencing Reads with Bowtie. *Curr Protoc Bioinform* **32**:11.7.1-11.7.14. doi:10.1002/0471250953.bi1107s32

Lanz MC, Dibitetto D, Smolka MB. 2019. DNA damage kinase signaling: checkpoint and repair at 30 years. *Embo J* **38**:e101801. doi:10.15252/embj.2019101801

Lao JP, Ulrich KM, Johnson JR, Newton BW, Vashisht AA, Wohlschlegel JA, Krogan NJ, Toczyski DP. 2018. The Yeast DNA Damage Checkpoint Kinase Rad53 Targets the Exoribonuclease, Xrn1. *G3 Genes Genomes Genetics* **8**:g3.200767.2018. doi:10.1534/g3.118.200767

Lee J, Shah M, Ballouz S, Crow M, Gillis J. 2020. CoCoCoNet: conserved and comparative co-expression across a diverse set of species. *Nucleic Acids Res* **48**:gkaa348-. doi:10.1093/nar/gkaa348

Love MI, Huber W, Anders S. 2014. Moderated estimation of fold change and dispersion for RNA-seq data with DESeq2. *Genome Biol* **15**:550. doi:10.1186/s13059-014-0550-8

Manfrini N, Gobbini E, Baldo V, Trovesi C, Lucchini G, Longhese MP. 2012. G1/S and G2/M Cyclin-Dependent Kinase Activities Commit Cells to Death in the Absence of the S-Phase Checkpoint. *Mol Cell Biol* **32**:4971–4985. doi:10.1128/mcb.00956-12

Oliveira FMB de, Harris MR, Brazauskas P, Bruin RAM de, Smolka MB. 2012. Linking DNA replication checkpoint to MBF cell-cycle transcription reveals a distinct class of G1/S genes. *The EMBO Journal* **31**:1798–1810. doi:10.1038/emboj.2012.27

Osborn AJ, Elledge SJ. 2003. Mrc1 is a replication fork component whose phosphorylation in response to DNA replication stress activates Rad53. *Gene Dev* **17**:1755–1767. doi:10.1101/gad.1098303

Pardo B, Crabbé L, Pasero P. 2017. Signaling pathways of replication stress in yeast. *FEMS Yeast Research* **17**. doi:10.1093/femsyr/fow101

Park D, Lee Y, Bhupindersingh G, Iyer VR. 2013. Widespread Misinterpretable ChIP-seq Bias in Yeast. *Plos One* **8**:e83506. doi:10.1371/journal.pone.0083506

Paulovich AG, Hartwell LH. 1995. A checkpoint regulates the rate of progression through S phase in S. cerevisiae in Response to DNA damage. *Cell* **82**:841–847. doi:10.1016/0092-8674(95)90481-6

Pellicioli A, Lucca C, Liberi G, Marini F, Lopes M, Plevani P, Romano A, Fiore PPD, Foiani M. 1999. Activation of Rad53 kinase in response to DNA damage and its effect in modulating phosphorylation of the lagging strand DNA polymerase. *The EMBO Journal* **18**:6561–6572. doi:10.1093/emboj/18.22.6561

Ramírez F, Dündar F, Diehl S, Grüning BA, Manke T. 2014. deepTools: a flexible platform for exploring deep-sequencing data. *Nucleic Acids Res* **42**:W187–W191. doi:10.1093/nar/gku365

Renard-Guillet C, Kanoh Y, Shirahige K, Masai H. 2014. Temporal and spatial regulation of eukaryotic DNA replication: From regulated initiation to genome-scale timing program. *Semin Cell Dev Biol* **30**:110–120. doi:10.1016/j.semcdb.2014.04.014

Saldivar JC, Cortez D, Cimprich KA. 2017. The essential kinase ATR: ensuring faithful duplication of a challenging genome. *Nature Publishing Group* **16**:1–15. doi:10.1038/nrm.2017.67

Sanz AB, García R, Rodríguez-Peña JM, Nombela C, Arroyo J. 2018. Slt2 MAPK association with chromatin is required for transcriptional activation of Rlm1 dependent genes upon cell wall stress. *Biochimica Et Biophysica Acta Bba - Gene Regul Mech* **1861**:1029–1039. doi:10.1016/j.bbagrm.2018.09.005

Sheu Y-J, Kinney JB, Lengronne A, Pasero P, Stillman B. 2014. Domain within the helicase subunit Mcm4 integrates multiple kinase signals to control DNA replication initiation and fork progression. *Proceedings of the National Academy of Sciences* **111**:E1899-908. doi:10.1073/pnas.1404063111

Sheu Y-J, Kinney JB, Stillman B. 2016. Concerted activities of Mcm4, Sld3, and Dbf4 in control of origin activation and DNA replication fork progression. *Genome Research* **26**:315–330. doi:10.1101/gr.195248.115

Sheu Y-J, Stillman B. 2006. Cdc7-Dbf4 phosphorylates MCM proteins via a docking site-mediated mechanism to promote S phase progression. *Mol Cell* **24**:101–113. doi:10.1016/j.molcel.2006.07.033

Sidorova JM, Breeden LL. 2003. Rad53 Checkpoint Kinase Phosphorylation Site Preference Identified in the Swi6 Protein of Saccharomyces cerevisiae. *Mol Cell Biol* **23**:3405–3416. doi:10.1128/mcb.23.10.3405-3416.2003

Siow CC, Nieduszynska SR, Müller CA, Nieduszynski CA. 2012. OriDB, the DNA replication origin database updated and extended. *Nucleic Acids Res* **40**:D682–D686. doi:10.1093/nar/gkr1091

Smolka MB, Albuquerque CP, Chen S, Zhou H. 2007. Proteome-wide identification of in vivo targets of DNA damage checkpoint kinases. *Proceedings of the National Academy of Sciences of the United States of America* **104**:10364–10369. doi:10.1073/pnas.0701622104

Smolka MB, Chen S, Maddox PS, Enserink JM, Albuquerque CP, Wei XX, Desai A, Kolodner RD, Zhou H. 2006. An FHA domain-mediated protein interaction network of Rad53 reveals its role in polarized cell growth. *The Journal of Cell Biology* **175**:743–753. doi:10.1083/jcb.200605081

Tercero JA, Longhese MP, Diffley JFX. 2003. A Central Role for DNA Replication Forks in Checkpoint Activation and Response. *Mol Cell* **11**:1323–1336. doi:10.1016/s1097-2765(03)00169-2

Teytelman L, Thurtle DM, Rine J, Oudenaarden A van. 2013. Highly expressed loci are vulnerable to misleading ChIP localization of multiple unrelated proteins. *Proc National Acad Sci* **110**:18602–18607. doi:10.1073/pnas.1316064110

Travesa A, Kuo D, Bruin RAM de, Kalashnikova TI, Guaderrama M, Thai K, Aslanian A, Smolka MB, Yates JR, Ideker T, Wittenberg C. 2012. DNA replication stress differentially regulates G1/S genes via Rad53-dependent inactivation of Nrm1. *The EMBO Journal* **31**:1811–1822. doi:10.1038/emboj.2012.28

Tsaponina O, Barsoum E, Aström SU, Chabes A. 2011. Ixr1 is required for the expression of the ribonucleotide reductase Rnr1 and maintenance of dNTP pools. *PLoS Genetics* **7**:e1002061. doi:10.1371/journal.pgen.1002061

Viggiani CJ, Aparicio OM. 2006. New vectors for simplified construction of BrdU-Incorporating strains of Saccharomyces cerevisiae. *Yeast* **23**:1045–1051. doi:10.1002/yea.1406

Yabuki N, Terashima H, Kitada K. 2002. Mapping of early firing origins on a replication profile of budding yeast. *Genes Cells* **7**:781–789. doi:10.1046/j.1365-2443.2002.00559.x

Zhao X, Georgieva B, Chabes A, Domkin V, Ippel JH, Schleucher J, Wijmenga S, Thelander L, Rothstein R. 2000. Mutational and Structural Analyses of the Ribonucleotide Reductase

Inhibitor Sml1 Define Its Rnr1 Interaction Domain Whose Inactivation Allows Suppression of mec1 and rad53 Lethality. *Mol Cell Biol* **20**:9076–9083. doi:10.1128/mcb.20.23.9076-9083.2000

Fig. 1

a Rad53 ChIP-seq in WT and mutant cells

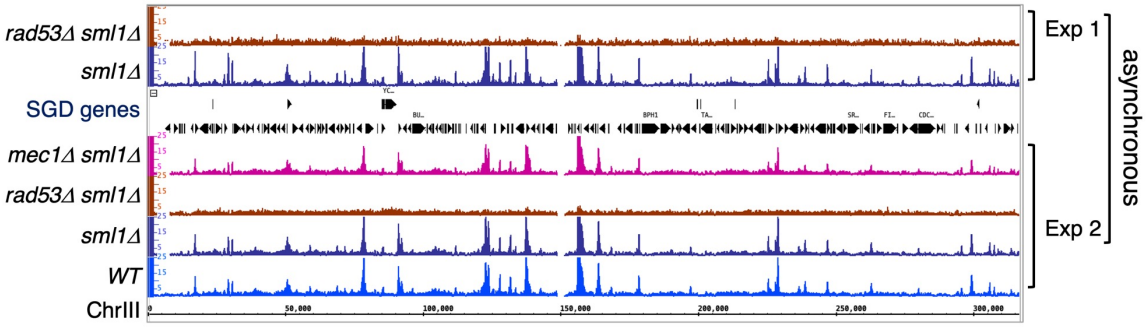

b

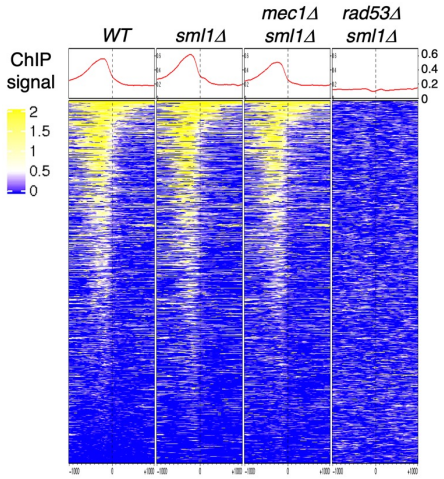

c

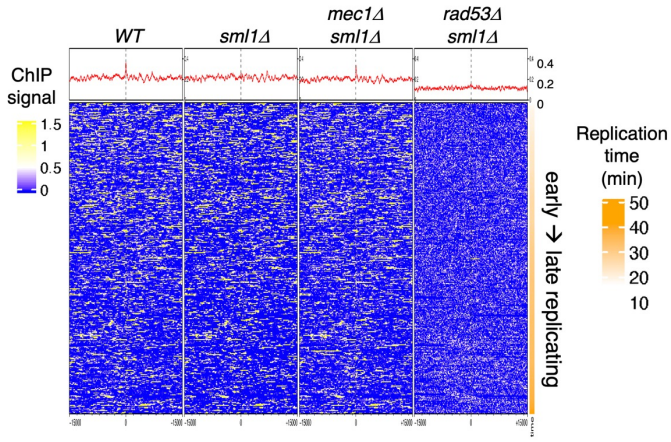

Fig. 2

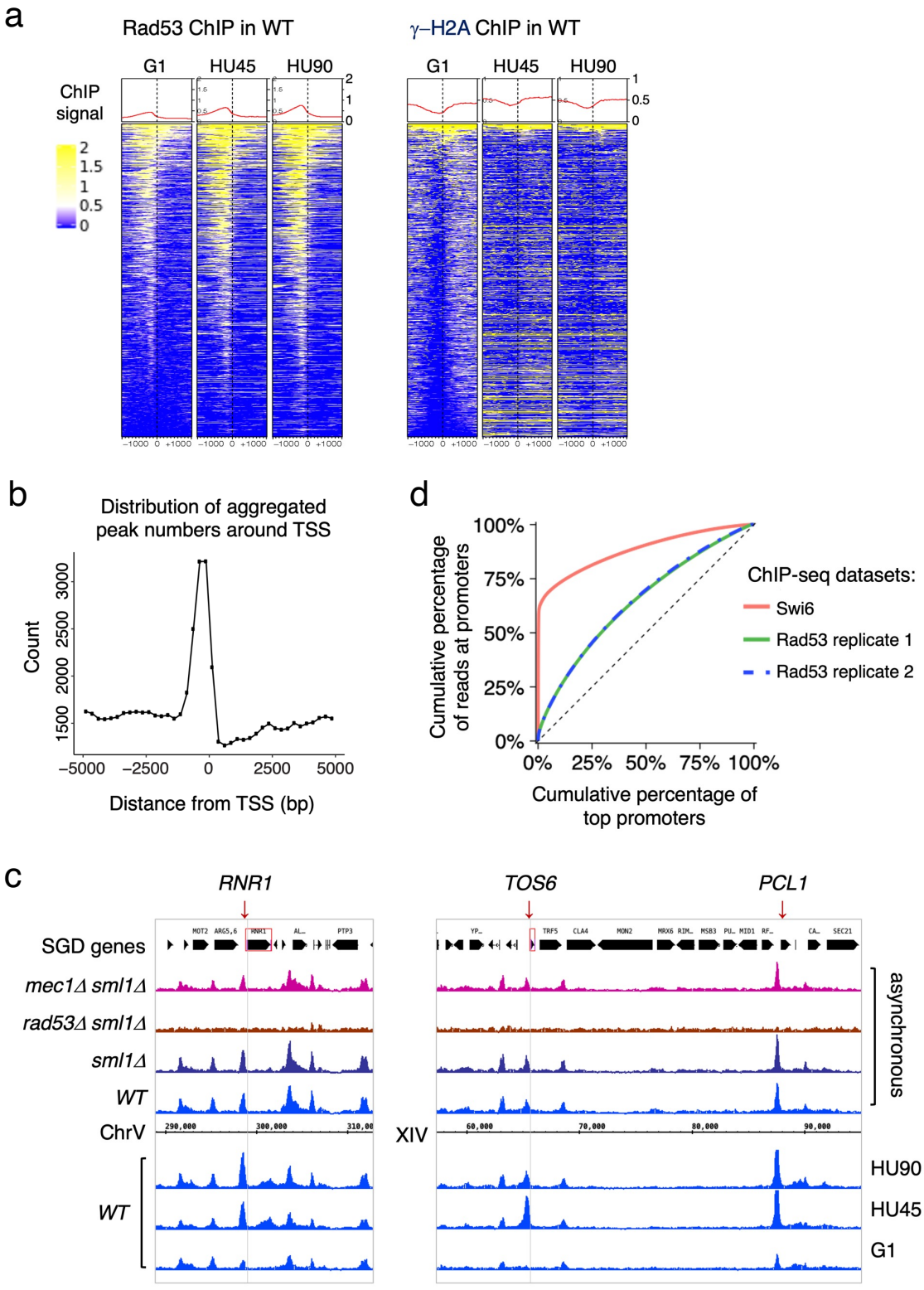
a
Rad53 ChIP in WT
γ–H2A ChIP in WT
G1
HU45
HU90
ChIP signal
2
1.5
1
0.5
0
−1000 0 +1000
b
Distribution of aggregated peak numbers around TSS
Count
1500 2000 2500 3000
−5000 −2500 0 2500 5000
Distance from TSS (bp)
d
Cumulative percentage of reads at promoters
100%
75%
50%
25%
0%
0% 25% 50% 75% 100%
Cumulative percentage of top promoters
ChIP-seq datasets:
Swi6
Rad53 replicate 1
Rad53 replicate 2
c
RNR1
TOS6
PCL1
SGD genes
mec1Δ sml1Δ
rad53Δ sml1Δ
sml1Δ
WT
ChrV
XIV
290,000
300,000
310,000
60,000
70,000
80,000
90,000
asynchronous
HU90
HU45
G1

Figure 2 – figure supplement 1

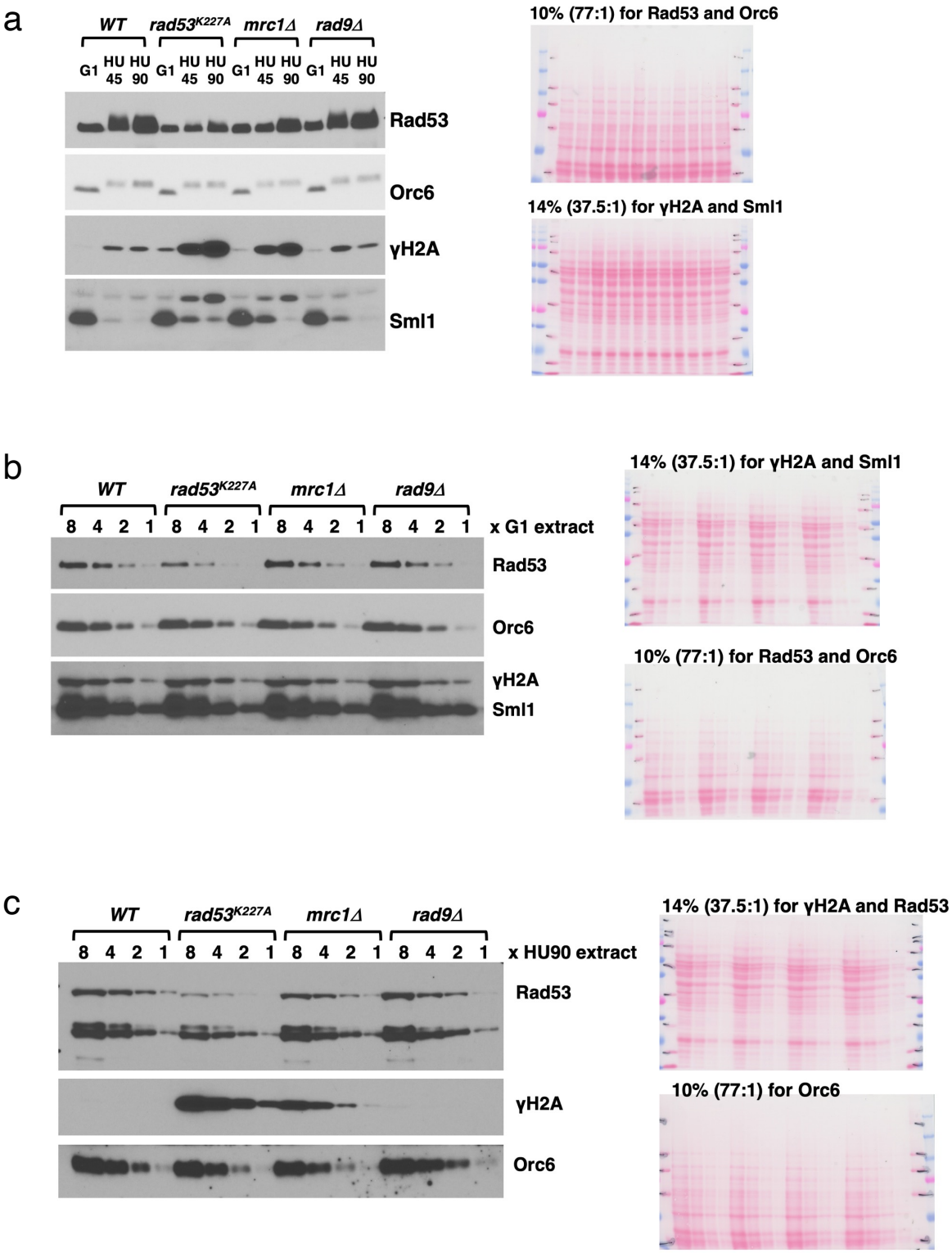

Figure 2 – figure supplement 2

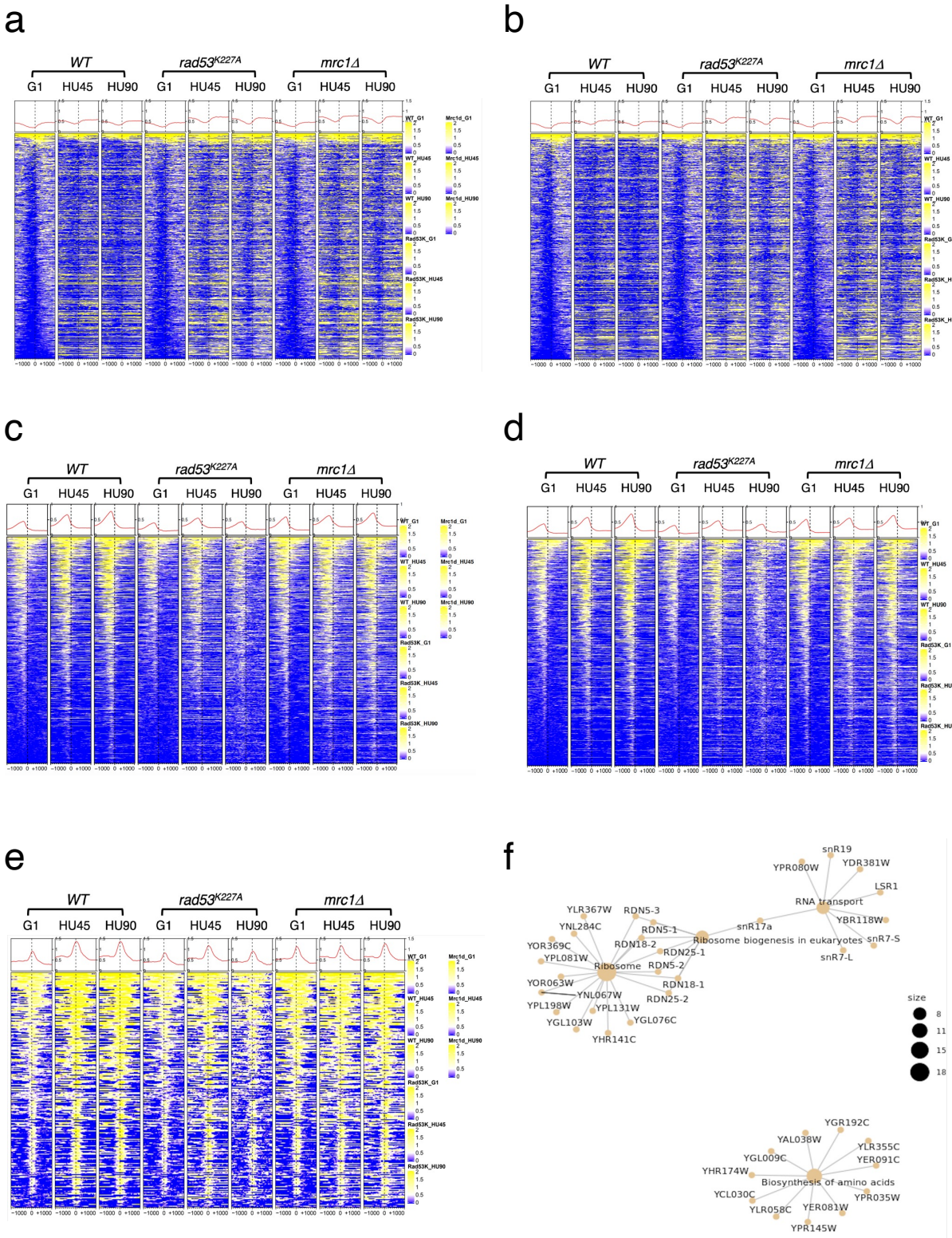

Figure 2 – figure supplement 3

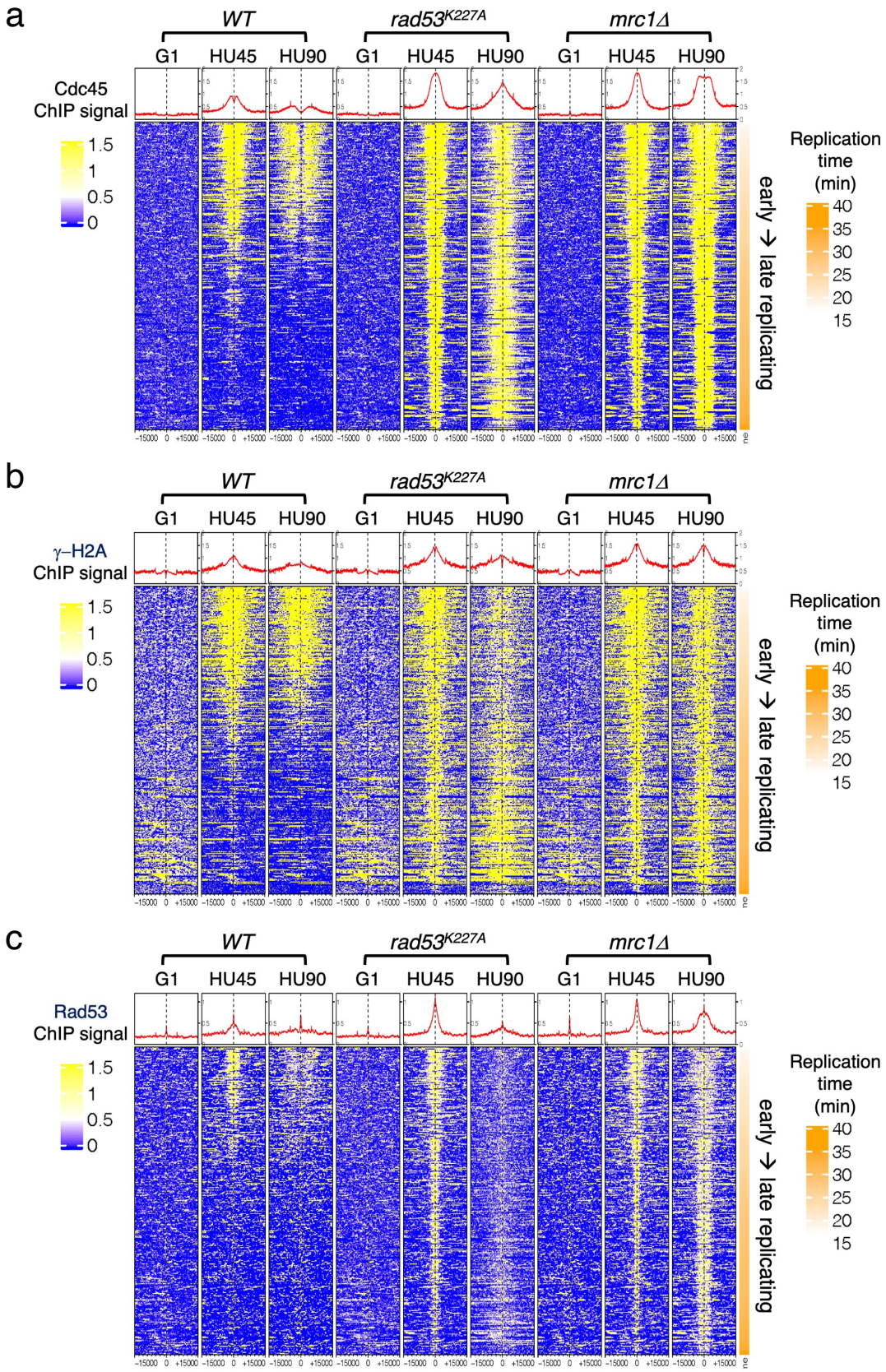

Fig. 3

a

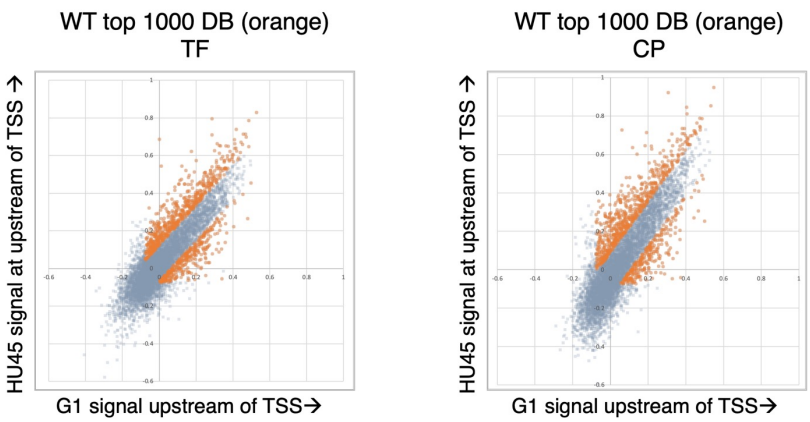

Increased Rad53 binding: 651
Decreased Rad53 binding: 349

Increased Rad53 binding: 703
Decreased Rad53 binding: 297

b

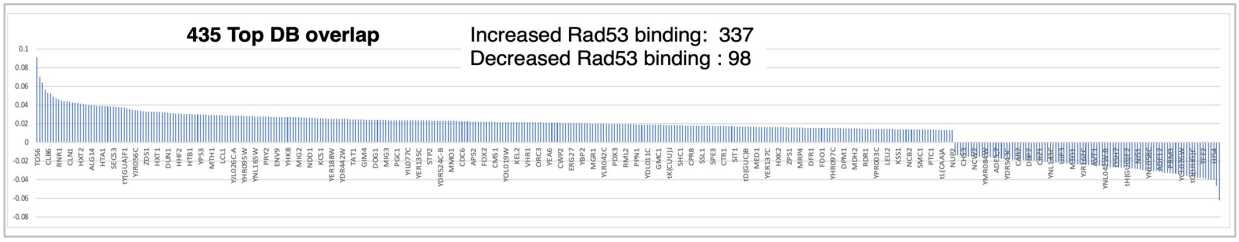

c

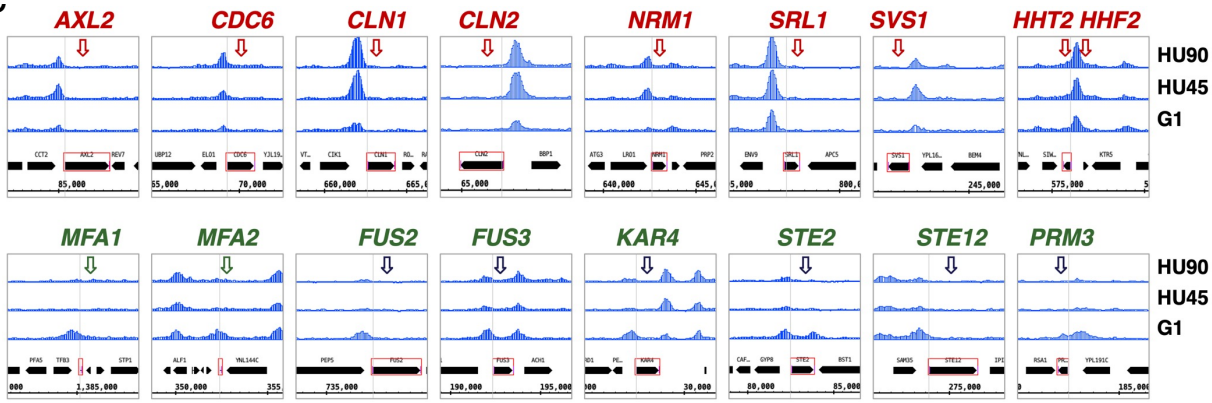

Fig. 4

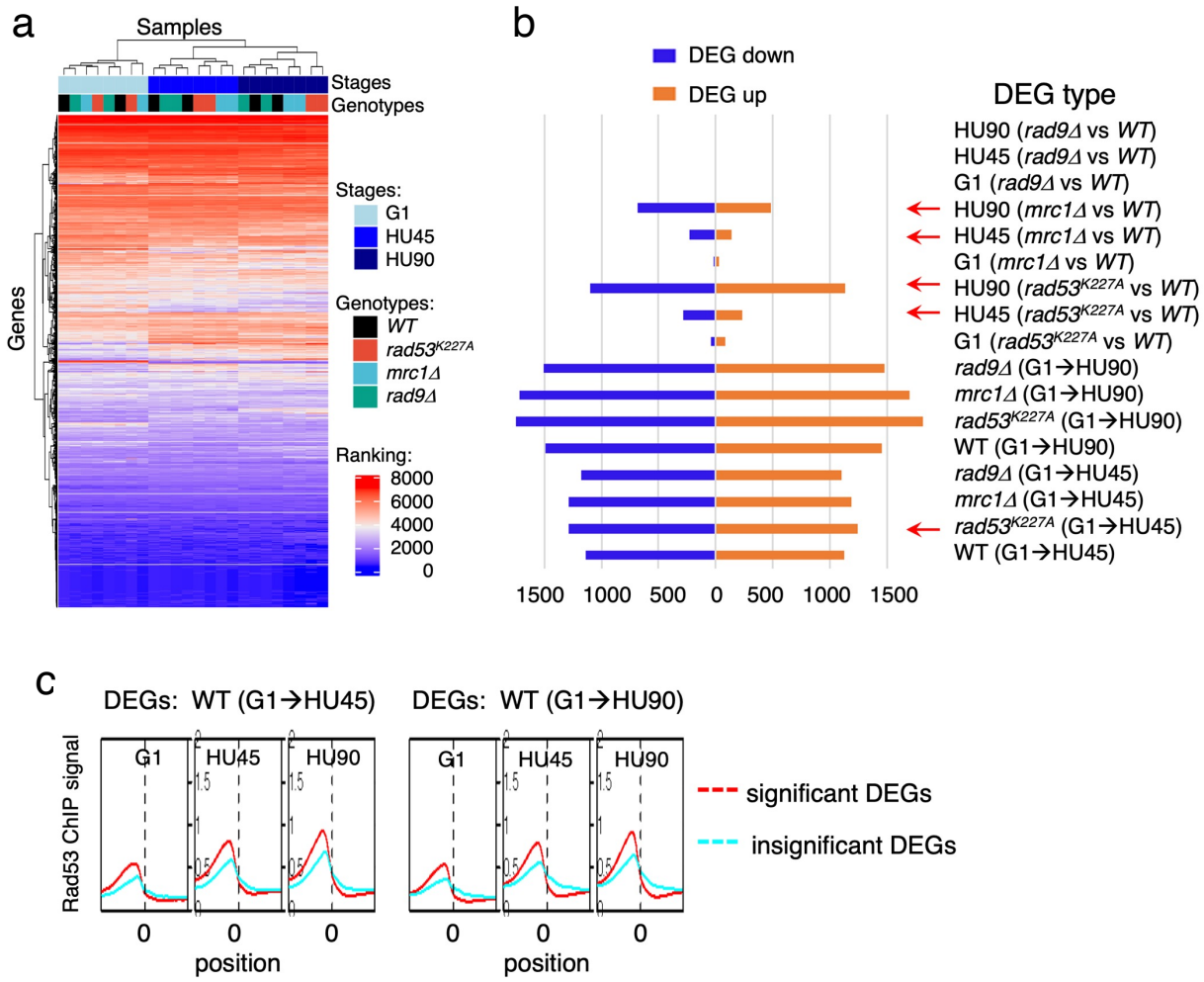
a
Samples
Stages
Genotypes
Genes
Stages:
G1
HU45
HU90
Genotypes:
WT
rad53K227A
mrc1Δ
rad9Δ
Ranking:
8000
6000
4000
2000
0
b
DEG down
DEG up
DEG type
HU90 (rad9Δ vs WT)
HU45 (rad9Δ vs WT)
G1 (rad9Δ vs WT)
HU90 (mrc1Δ vs WT)
HU45 (mrc1Δ vs WT)
G1 (mrc1Δ vs WT)
HU90 (rad53K227A vs WT)
HU45 (rad53K227A vs WT)
G1 (rad53K227A vs WT)
rad9Δ (G1→HU90)
mrc1Δ (G1→HU90)
rad53K227A (G1→HU90)
WT (G1→HU90)
rad9Δ (G1→HU45)
mrc1Δ (G1→HU45)
rad53K227A (G1→HU45)
WT (G1→HU45)
1500 1000 500 0 500 1000 1500
c
DEGs: WT (G1→HU45)
DEGs: WT (G1→HU90)
Rad53 ChIP signal
G1
HU45
HU90
position
significant DEGs
insignificant DEGs

Figure 4 – figure supplement 1

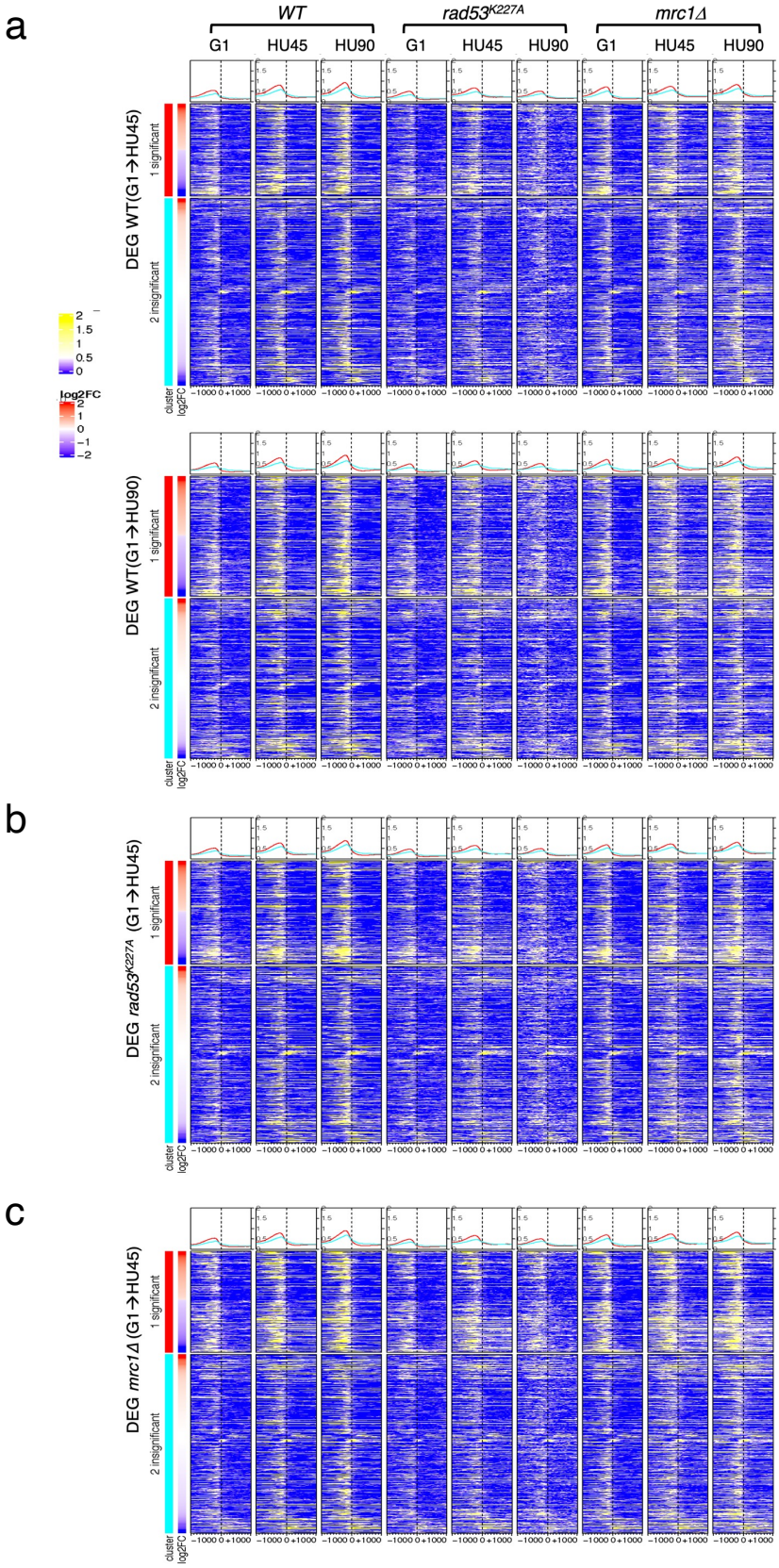

Fig. 5

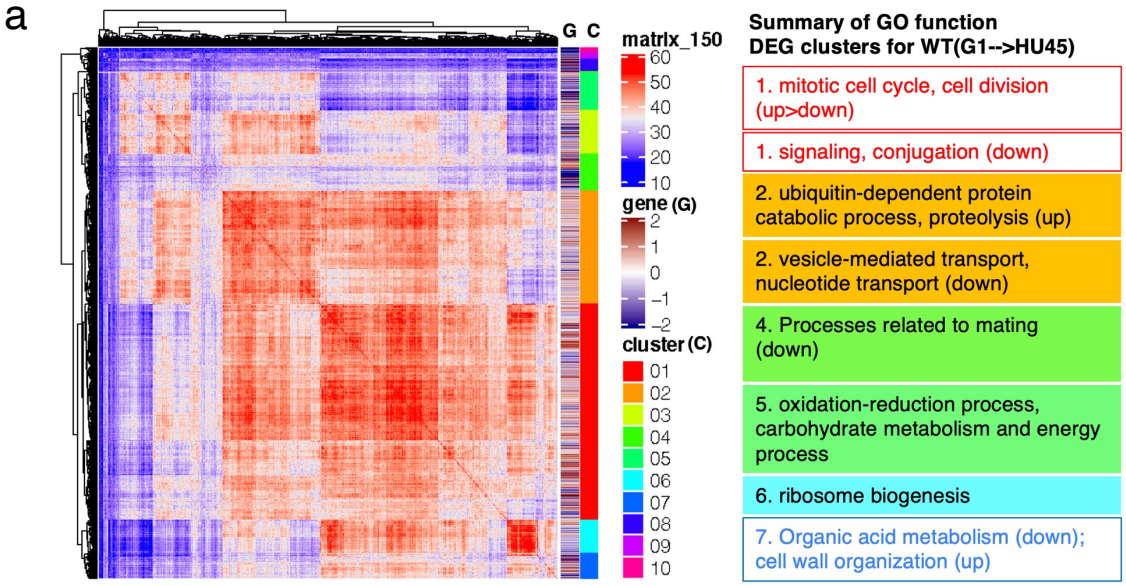
a
G C
matrix_150
60
50
40
30
20
10
gene (G)
2
1
0
−1
−2
cluster (C)
01
02
03
04
05
06
07
08
09
10
Summary of GO function
DEG clusters for WT(G1-->HU45)
1. mitotic cell cycle, cell division (up>down)
1. signaling, conjugation (down)
2. ubiquitin-dependent protein catabolic process, proteolysis (up)
2. vesicle-mediated transport, nucleotide transport (down)
4. Processes related to mating (down)
5. oxidation-reduction process, carbohydrate metabolism and energy process
6. ribosome biogenesis
7. Organic acid metabolism (down); cell wall organization (up)

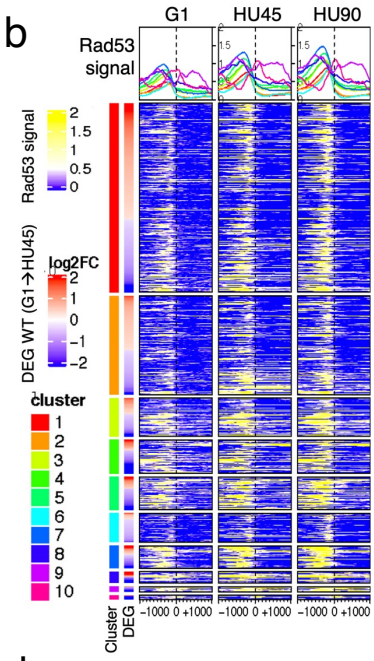
b
G1
HU45
HU90
Rad53 signal
Rad53 signal
2
1.5
1
0.5
0
DEG WT (G1→HU45)
log2FC
2
1
0
−1
−2
cluster
1
2
3
4
5
6
7
8
9
10
Cluster
DEG
−1000 0 +1000
−1000 0 +1000
−1000 0 +1000

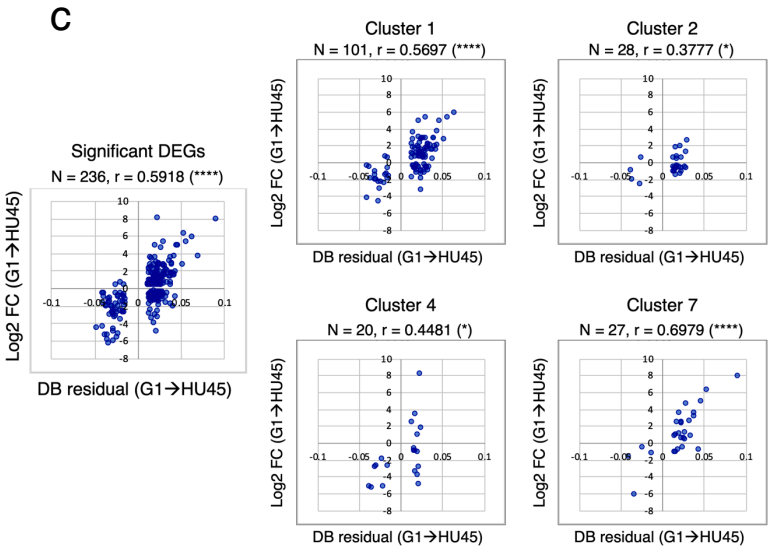
c
Significant DEGs
N = 236, r = 0.5918 (****)
Log2 FC (G1→HU45)
DB residual (G1→HU45)
Cluster 1
N = 101, r = 0.5697 (****)
Cluster 2
N = 28, r = 0.3777 (*)
Cluster 4
N = 20, r = 0.4481 (*)
Cluster 7
N = 27, r = 0.6979 (****)

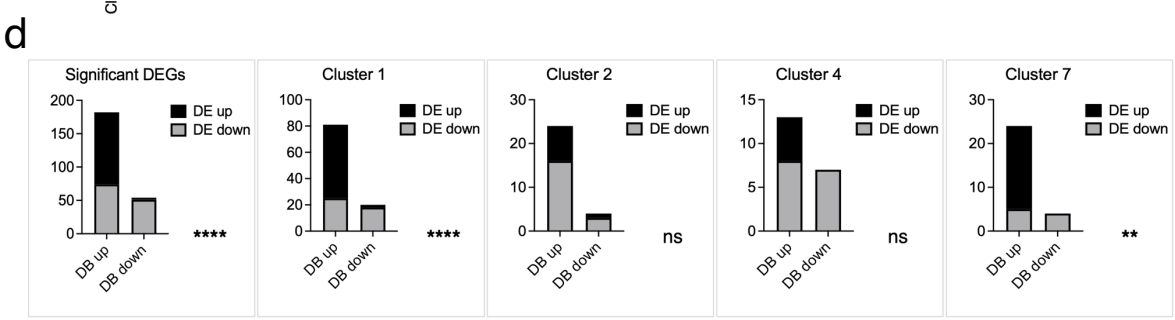
d
Significant DEGs
Cluster 1
Cluster 2
Cluster 4
Cluster 7
DE up
DE down
DB up
DB down
****
****
ns
ns
**

Fig. 6

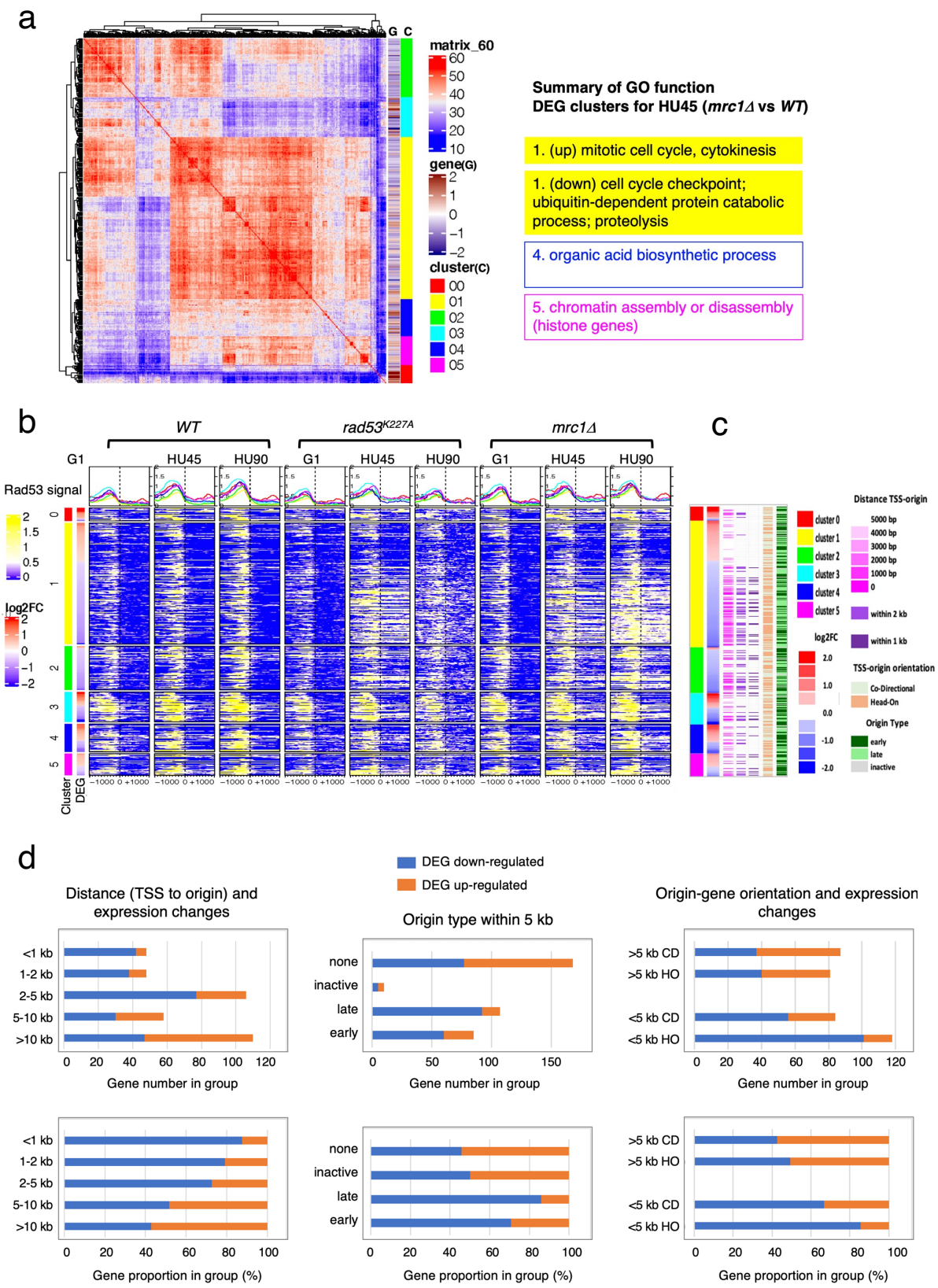
a
G C
matrix_60
60
50
40
30
20
10
gene(G)
2
1
0
−1
−2
cluster(C)
00
01
02
03
04
05
Summary of GO function
DEG clusters for HU45 (mrc1Δ vs WT)
1. (up) mitotic cell cycle, cytokinesis
1. (down) cell cycle checkpoint; ubiquitin-dependent protein catabolic process; proteolysis
4. organic acid biosynthetic process
5. chromatin assembly or disassembly (histone genes)
b
WT
rad53K227A
mrc1Δ
G1
HU45
HU90
Rad53 signal
log2FC
Cluster
DEG
c
cluster 0
cluster 1
cluster 2
cluster 3
cluster 4
cluster 5
Distance TSS-origin
5000 bp
4000 bp
3000 bp
2000 bp
1000 bp
0
within 2 kb
within 1 kb
TSS-origin orientation
Co-Directional
Head-On
Origin Type
early
late
inactive
d
DEG down-regulated
DEG up-regulated
Distance (TSS to origin) and expression changes
Origin type within 5 kb
Origin-gene orientation and expression changes
<1 kb
1-2 kb
2-5 kb
5-10 kb
>10 kb
none
inactive
late
early
>5 kb CD
>5 kb HO
<5 kb CD
<5 kb HO
Gene number in group
Gene proportion in group (%)

Figure 6 – figure supplement 1

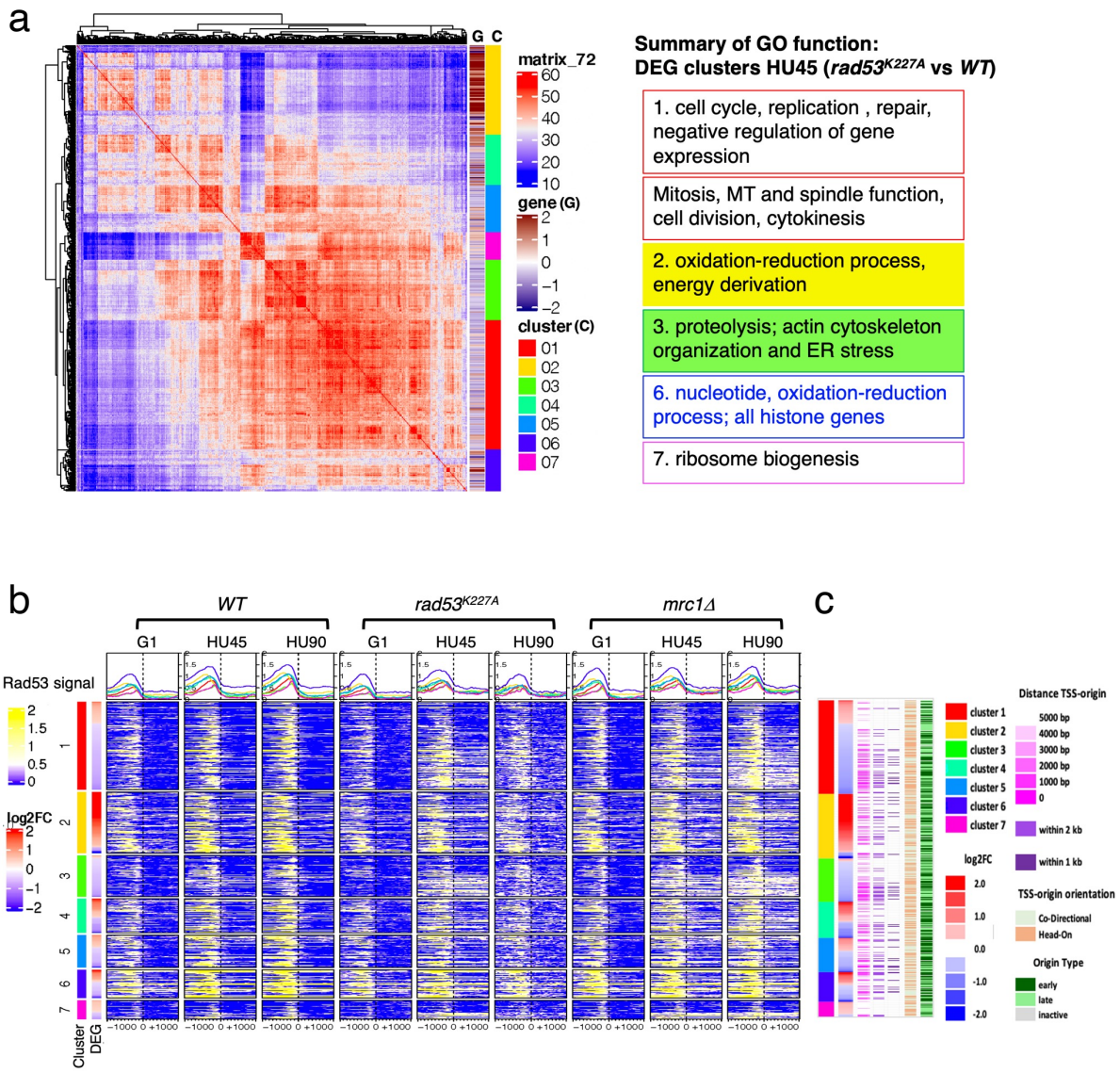

Fig. 7

a

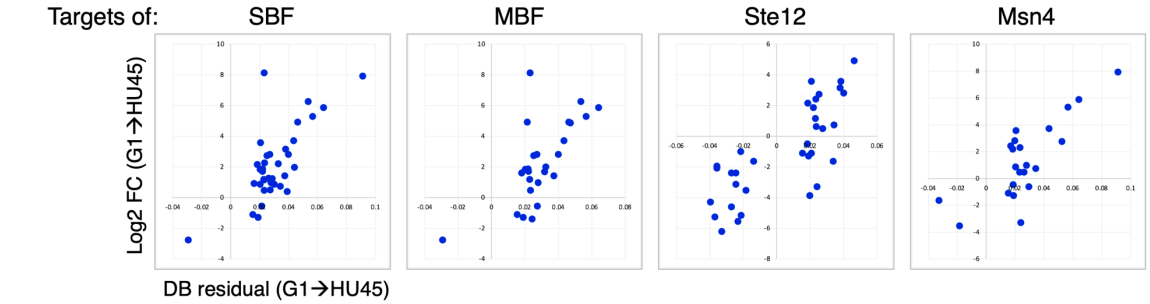

	SBF	MBF	Ste12	Msn4
Spearman r	r = 0.5498 (***)	r = 0.5925 (**)	r = 0.7672 (****)	r = 0.616 (**)
	N = 36	N = 26	N = 34	N = 22

Fisher's exact test for enrichment of TF targets

p < 1E-15	p < 1E-15	p < 1E-15	p = 1.18E-06

b

Targets of SBF in 236 DB

Fig. 8

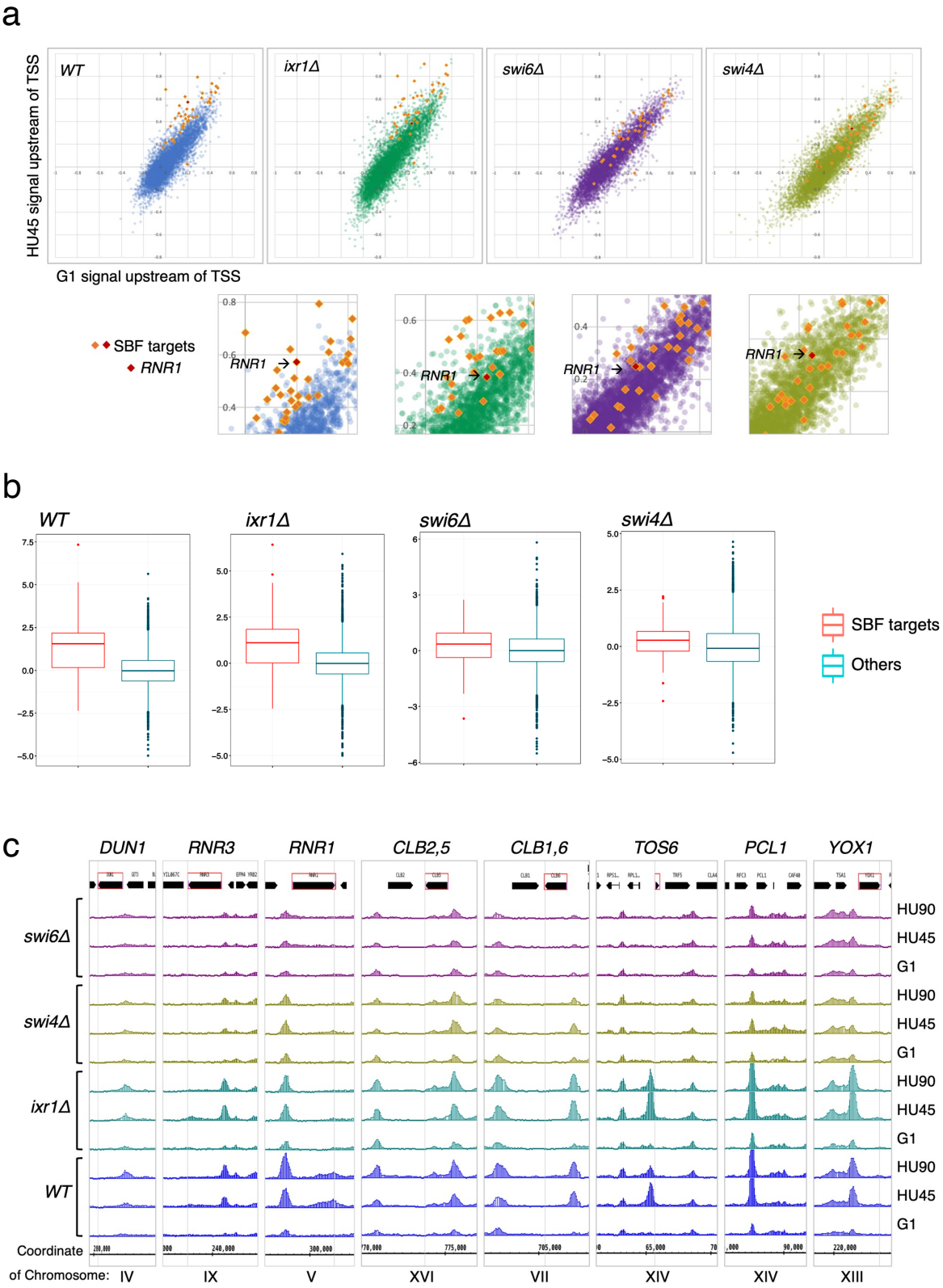
a
WT
ixr1Δ
swi6Δ
swi4Δ
HU45 signal upstream of TSS
G1 signal upstream of TSS
SBF targets
RNR1
b
WT
ixr1Δ
swi6Δ
swi4Δ
SBF targets
Others
c
DUN1
RNR3
RNR1
CLB2,5
CLB1,6
TOS6
PCL1
YOX1
swi6Δ
swi4Δ
ixr1Δ
WT
HU90
HU45
G1
Coordinate of Chromosome:
IV
IX
V
XVI
VII
XIV
XIV
XIII